Reactive Oxygen Species Responsive Nanoprodrug to Treat Intracranial Glioblastoma

Bong-Seop Lee, Takayuki Amano, Hong Qiang Wang, Joe L. Pantoja, Chi Woo Yoon, Christopher J. Hanson, Rina Amatya, Allen Yen, Keith L. Black, and John S. Yu*

Department of Neurosurgery, Cedars-Sinai Medical Center, 8631 West Third Street, Suite 800 East, Los Angeles, California 90048, United States

ABSTRACT Chemotherapy for intracranial gliomas is hampered by limited delivery of therapeutic agents through the blood brain barrier (BBB). An optimal therapeutic agent for brain tumors would selectively cross the BBB, accumulates in the tumor tissue and be activated from an innocuous prodrug within the tumor. Here we show brain tumor-targeted delivery and therapeutic efficacy of a nanometer-sized prodrug (nanoprodrug) of camptothecin (CPT) to treat experimental glioblastoma multiforme (GBM). The CPT nanoprodrug was prepared using spontaneous nanoemulsification of a biodegradable, antioxidant CPT prodrug and α-tocopherol. The oxidized nanoprodrug was activated more efficiently than nonoxidized nanoprodrug, suggesting enhanced therapeutic efficacy in the oxidative tumor microenvironment. The *in vitro* imaging of U-87 MG glioma cells revealed an efficient intracellular uptake of the nanoprodrug *via* direct cell membrane penetration rather than *via* endocytosis. The *in vivo* study in mice demonstrated that the CPT nanoprodrug passed through the BBB and specifically accumulated in brain tumor tissue, but not in healthy brain tissue and other organs. The accumulation preferably occurred at the periphery of the tumor where cancer cells are most actively proliferating, suggesting optimal therapeutic efficacy of the nanoprodrug. The nanoprodrug was effective in treating subcutaneous and intracranial tumors. The nanoprodrug inhibited subcutaneous tumor growth more than 80% compared with control. The median survival time of mice implanted with an intracranial tumor increased from 40.5 days for control to 72.5 days for CPT nanoprodrug. This nanoprodrug approach is a versatile method for developing therapeutic nanoparticles enabling tumor-specific targeting and treatment. The nontoxic, tumor-specific targeting properties of the nanoprodrug system make it a safe, low cost, and versatile nanocarrier for pharmaceuticals, imaging agents, and diagnostic agents.

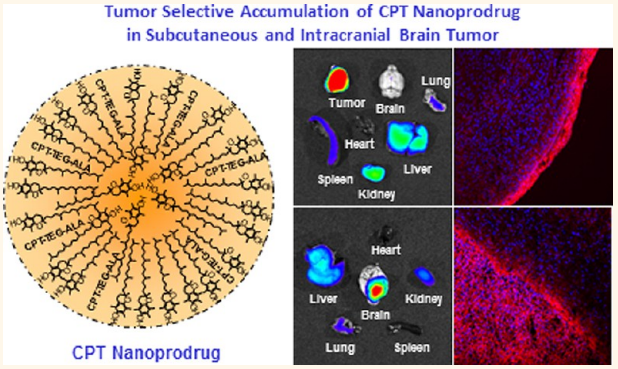

KEYWORDS: glioblastoma · nanoprodrug · drug delivery · targeted cancer therapy · EPR effect · nonendosomal cellular uptake · nanoplatform

Glioblastoma is the most common and aggressive type of malignant primary brain tumor in adults. Despite advances in neurosurgical intervention, radiation therapy, and chemotherapy, the median survival for glioblastoma remains less than15 months after diagnosis and tumors recur usually within 6 to 12 months of chemoradiation initiation.[1,2] The treatment of intracranial glioma is limited by the inability to deliver chemotherapeutics at efficacious levels to the site of tumor.[3] The blood–brain barrier (BBB) is a tightly regulated interface between the circulating blood and brain tissues formed by brain microvascular endothelial cells. The BBB maintains the homeostasis of the highly sensitive central nervous system (CNS) and protects the brain from neurotoxic substances prevalent in the peripheral circulatory system.[4] The BBB prevents free diffusion of most foreign molecules including therapeutic agents except for those that are small, uncharged, and lipid-soluble.[5] This remains the major obstacle for drug delivery into the brain. However, integrity of the BBB is severely compromised by many diseases in the brain, including brain tumors, neurodegenerative diseases, and traumatic brain injury (TBI).[6–8] Vigorous tumor growth leads to induction of unregulated angiogenesis, resulting in defective vasculature with large pores and high permeability. This allows

* Address correspondence to john.yu@cshs.org.

Received for review October 15, 2012 and accepted March 28, 2013.

Published online March 28, 2013
10.1021/nn400347j

certain macromolecules and nanoparticles to penetrate through the BBB into the tumor and, due to the defective lymphatic drainage system in the tumor tissue, accumulate at therapeutically effective concentrations.[9] This phenomenon is termed the enhanced permeability and retention (EPR) effect, and it grants the opportunity for passive tumor-specific targeting with macromolecular drugs and nanocarriers.[10]

Camptothecin (CPT), a pentacyclic alkaloid extracted from the bark of the Chinese tree *Camptotheca acuminate*, has been proved for its anticancer activity *in vitro* and *in vivo* animal solid tumors.[11,12] The major problem encountered with CPT is its extremely low solubility in an aqueous environment. Its carboxylate form is more water-soluble, but the loss of the lactone form resulted in the loss of its anticancer efficacy.[13] Furthermore, the use of the hydrophilic carboxylate form was associated with severe, unpredictable side effects.[14−16] Following the discovery that CPT acts through binding to topoisomerase I and inducing irreversible double-strand DNA breaks,[17,18] investigators have sought to improve the therapeutic efficacy of CPT by reducing its nonspecific toxicity and increasing its water solubility. The efforts to find more water-soluble analogues of CPT has led to the development of small molecule analogues such as topotecan and irinotecan,[13] and many CPT-polymer conjugates such as poly(ethylene glycol)-CPT,[19] poly(L-glutamic acid)-CPT,[20] and dextran-CPT.[21]

Research in the field of cancer therapy using nanostructured materials has been receiving significant attention from the pharmaceutical industry due to their potential for precise targeting, improved tolerability, and drug efficacy.[22] One of the major advantages of nanostructured materials is that hydrophobic therapeutics can be transported more efficiently in the aqueous physiological environment when integrated into stable nanostructures.[23] In an effort to overcome the problems for delivery of CPT-based chemotherapeutics, nanoparticles loaded with CPT analogues have received significant attention in recent years. Noble *et al.* used nanometer-sized liposomes for delivery of irinotecan, which resulted in a higher drug residence time in tissue, reduced toxicity, and effective treatment of brain tumor.[24] Koizumi *et al.* developed therapeutic polymeric micelles by direct incorporation of the active metabolite of irinotecan, SN-38,[25] into the micelles.[26] The above reports demonstrated the strategy and feasibility to overcome the intrinsic problems of CPT-based drugs and enhance the therapeutic efficacy by using nanoparticles as tumor-targeting drug delivery vehicles.

In our efforts to develop a new tumor-targeting therapeutic nanoparticle, we have designed a nanometer-sized prodrug (nanoprodrug) by combining the concept of a prodrug with a nanoscale drug delivery system. In our previous study, we synthesized a new CPT prodrug and prepared a nanoprodrug of CPT using spontaneous nanoemulsification.[27] In this study, we demonstrate that the nanoprodrug can cross the BBB in brain tumor (also called the blood−brain tumor barrier, BTB), passively accumulate in the brain tumor tissue *via* the EPR effect, and exhibit antitumor efficacy in experimental animal models with subcutaneous or intracranial human glioblastomas.

RESULTS AND DISCUSSION

Preparation and Characterization of CPT Nanoprodrug. Brain tumors are one of the most deadly and difficult to treat and cure. This is largely due to the failure to deliver sufficient amount of drugs through the BBB into the tumor tissue. Nanometer-sized materials have drawn considerable attention for their potential application as a therapeutic platform in oncology. Polymer nanoparticles have been widely used to overcome the problems associated with drug solubility and stability and to target tumors by exploiting the EPR effect-based passive drug targeting and accumulation.[28] In addition to this passive targeting, active targeting using ligands or antibodies directed against selected tumor targets increases selectivity for cancers. McCarron *et al.* developed a CPT-loaded polymer nanoparticles with a layer of antibodies to actively target tumor cells.[29] The improved efficacy of this nanoparticle was explained by the increased intracellular delivery of the nanoparticles resulting from the active antibody targeting toward Fas receptor on the surface of tumor cells. Liposomes and polymeric micelles have been reported to significantly increase the therapeutic efficacy compared with free drugs. The liposomal CPT-based drugs have been shown to increase the stability of the drugs, accumulate to higher levels in tumors, and have a longer overall residence time than free drugs.[30] To facilitate the delivery into the brain, CPT-loaded PLGA polymer nanoparticles[31] and liposomal CPT-11[24] were infused *via* convection-enhanced delivery (CED) to a defined location in the brain, which improved drug distribution in the brain parenchyma. However, for the treatment of brain tumors, the *in vivo* efficacy of drug-loaded nanoparticles may be compromised by their inefficiency in crossing the BBB, the lack of brain tumor-specific targeting ability, and insufficient accumulation and retention within the tumor tissue. Our goal was to develop a brain tumor-targeted delivery system for CPT and CPT analogues using a nanoparticle that is capable of passive accumulation *via* the EPR effect without using active targeting ligands. While most of the efforts to improve bioavailability and therapeutic efficacy of CPT-based drugs have strived to develop a more water-soluble analogue of CPT, we aimed to design a more hydrophobic CPT prodrug that can be transformed into a nanoprodrug by spontaneous hydrophobic assembly. In order to obtain a hydrophobic, biodegradable prodrug, we first synthesized CPT prodrug from CPT, tetra(ethylene glycol) (TEG) spacer, and

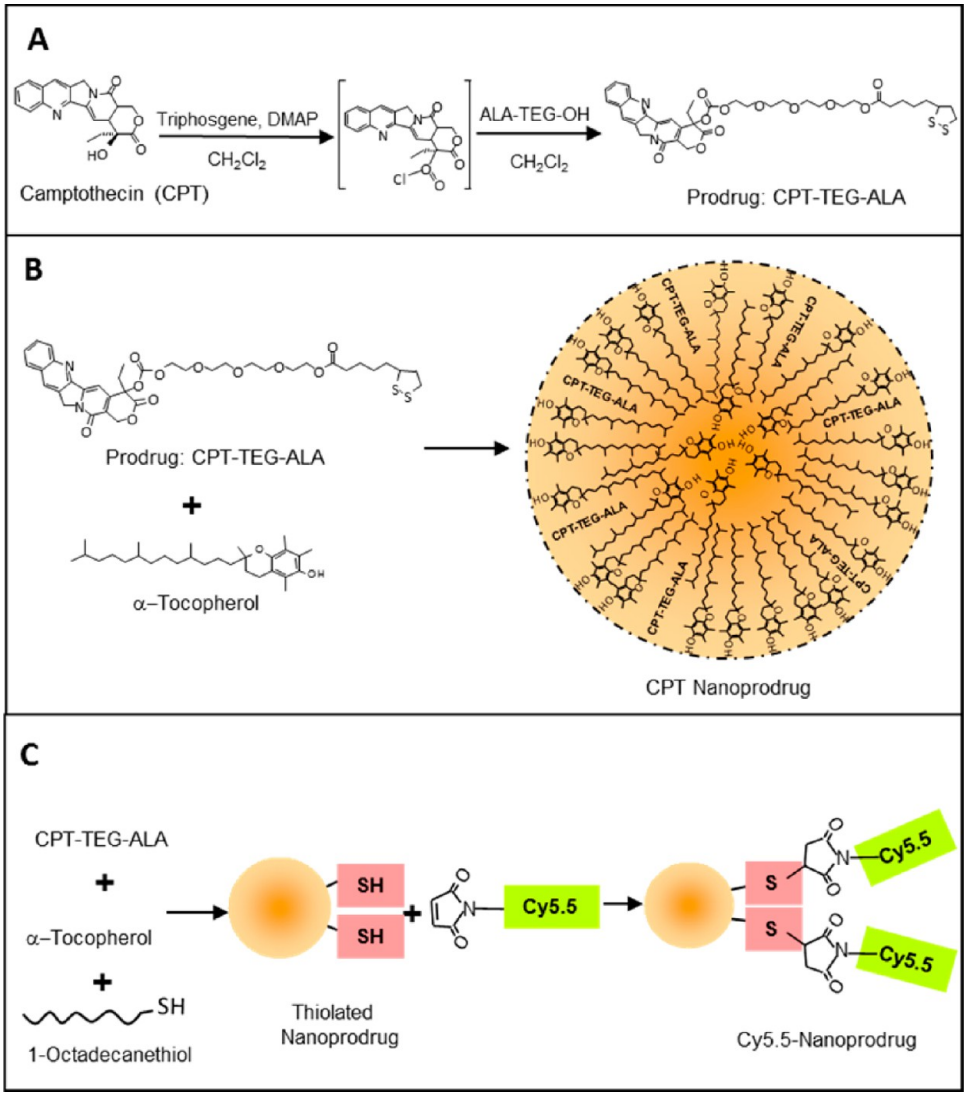

Figure 1. Preparation of camptothecin (CPT) prodrug and nanoprodrug. (A) Free CPT is incorporated with α-lipoic acid (ALA) and tetra(ethylene glycol) (TEG) into prodrug CPT-TEG-ALA *via* ester and carbonate bonds. (B) CPT prodrug and α-tocopherol (Toco) undergo spontaneous emulsification into CPT-TEG-ALA/Toco nanoprodrug (CPT nanoprodrug). (C) Thiol groups are incorporated into the nanoprodrug by addition of 1-octadecanethiol. Nanoprodrug is then fluorescently labeled by conjugation of Cy5.5-maleimide to thiol moiety of 1-octadecanethiol on the surface of the nanoprodrug.

α-lipoic acid (ALA) by introducing biodegradable carbonate and ester bonds (Figure 1A).

The biodegradable bonds ensure that the prodrug molecules break down hydrolytically or enzymatically by esterase. Spontaneous emulsification of the prodrug and α-tocopherol into the nanoprodrug abates problems associated with free delivery of the highly hydrophobic prodrug (Figure 1B). The resulting nanoprodrug attains a stable structure that can exploit the EPR effect for tumor specific entry and retention. Interestingly, in contrast to CPT prodrug, CPT was not incorporated into α-tocopherol nanoemulsion. Most CPT precipitated during the emulsification process. The results highlight the influence of molecular structure and intermolecular interaction on the formation of stable nanostructures. The nanoprodrug strategy is an example of constructing therapeutic nanostructures using molecular self-assembly. Molecular self-assembly is defined as the spontaneous association of molecules under equilibrium condition into stable, structurally well-defined aggregates joined by noncovalent bonds.[32] The initiation or stability of self-assembly depends on the physical/chemical properties of the components in the system, such as structure, shape, charge, polarization, magnetic dipole, mass, *etc.*, which determine the noncovalent interaction (van der Waals, electrostatic and hydrophobic interaction, hydrogen and coordination bonds) among them.[33] The modification of CPT to CPT-TEG-ALA prodrug resulted in dramatic changes in physical and chemical properties of the molecule: CPT has a slightly yellowish powder form, while CPT prodrug is sticky yellow oil similar to α-tocopherol. The solubility of CPT in acetone is ~0.1 mg/mL, while it is >1.0 g/mL for CPT prodrug. These changes are believed

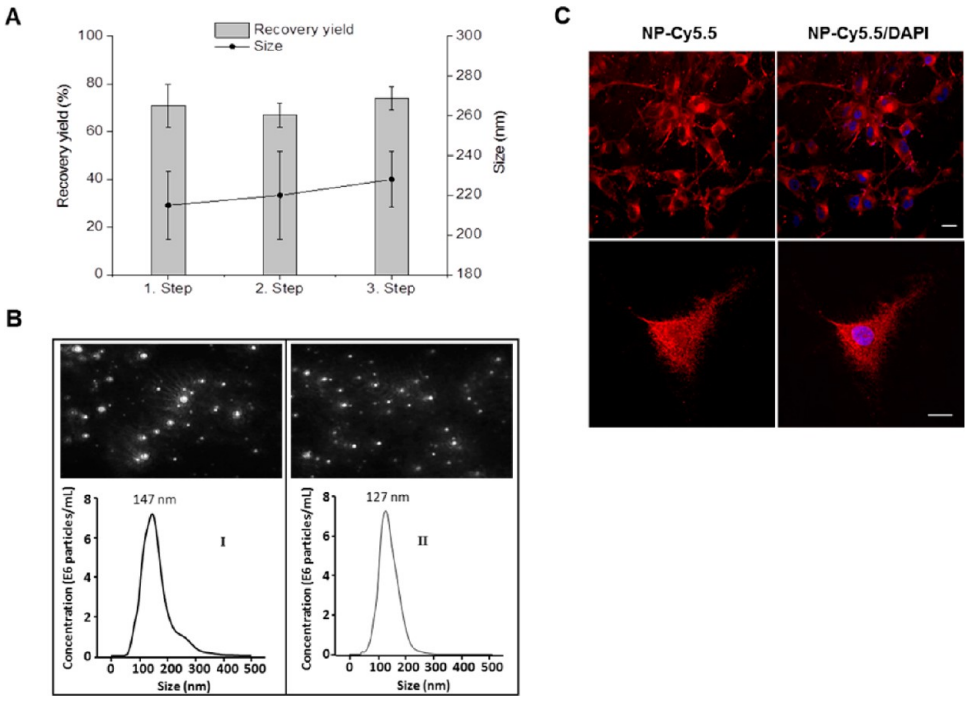

Figure 2. (A) Recovery yield of CPT prodrug and size of nanoprodrug measured by dynamic light scattering (DLS) after the first, second, and third step of spontaneous emulsification. The mean diameter and standard deviation were calculated from the measurements of three separate preparations. (B) Visualization and size distribution of CPT nanoprodrug (I) and α-tocopherol (Toco) nanosuspension (II) obtained from nanoparticle tracking analysis (NTA).[35] (C) *In vitro* cellular uptake of CPT nanoprodrug into U-87 MG glioma cells after a 5 h incubation visualized by fluorescence detection of Cy5.5 functionalized nanoprodrug as determined by laser confocal microscopy. Scale bars, 20 μm.

to be caused by introducing the TEG spacer. It is plausible that the flexible TEG spacer facilitates optimal spatial arrangement of CPT prodrug and α-tocopherol and, thus, the hydrogen bond formation between the oxygen atoms of TEG and the hydroxyl proton of α-tocopherol. The above results suggest that the intermolecular forces between CPT prodrug and α-tocopherol favors the formation of mixed self-assembly (nanoprodrug), while CPT molecule acts against the formation of self-assembly with α-tocopherol. The hydrophobic interaction between the prodrug and α-tocopherol molecules stabilizes the nanoprodrug in an aqueous environment, which maintains the structural integrity of the nanostructures. The hydrophobic nature of the prodrug and its strong hydrophobic assembly with α-tocopherol may reduce its activation in aqueous physiologic condition and this would reduce its therapeutic efficacy. However, the transformation into the nanoprodrug generates abundant reactive surface area where the prodrugs are activated upon contact with biological molecules. This increased interaction increases the rate of prodrug activation and thus improves therapeutic efficacy.[34] To visualize the *in vivo* delivery, we aimed to fluorescently label the nanoprodrug. We first prepared nanoprodrug containing 1-octadecanethiol. Cy5.5 maleimide was conjugated to the thiol groups on the surface of the nanoprodrug (Figure 1C).

In our previous report, we developed a single-step spontaneous emulsification method for nanoprodrug preparation.[27] In order to increase the concentration of the prodrug in nanoprodrug, we applied the three-step emulsification method as described in the Materials and Methods. The recovery yield was about 70% throughout the three-step process (Figure 2A). The concentration of the recovered prodrug CPT-TEG-ALA was 652, 1239, and 2122 μM after the first, second, and third step, respectively. The hydrodynamic size measured by the dynamic light scattering (DLS) using a Coulter N4-Plus Submicrometer Particle Sizer was 215 ± 17 nm (PDI = 0.18), 220 ± 22 nm (PDI = 0.14), and 228 ± 14 nm (PDI = 0.25) after the first, second, and third emulsification step, respectively. Notably, the amount of recovered prodrug CPT-TEG-ALA after the second and third emulsification step were approximately twice and three times as much as the amount of the single-step procedure, whereas the size increased only slightly after each additional step. The polydispersity index (PDI) of all nanoprodrugs remained below 0.3. This multistep procedure of spontaneous emulsification represents a rapid, reliable, and reproducible method for the preparation of concentrated nanoprodrug.

In this study, we also applied the nanoparticle tracking and analysis (NTA) technique to visualize the nanoprodrug in a suspension. Figure 2B shows that the size of the CPT nanoprodrug is larger than the nanosuspension prepared from α-tocopherol (Toco). The average size of the CPT-nanoprodrug was 147 nm when calculated using NTA, which was significantly

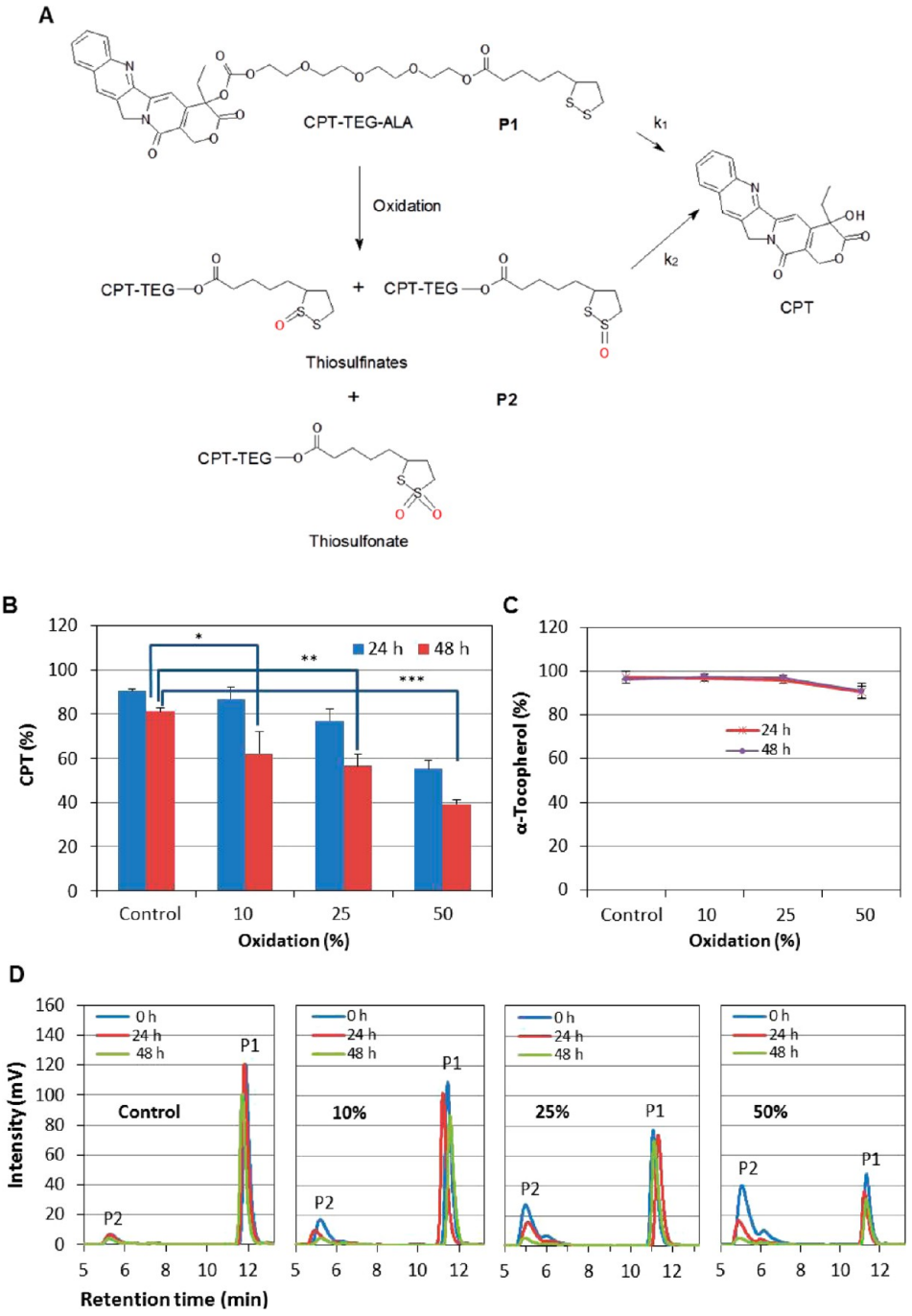

Figure 3. Oxidation-sensitive prodrug activation from CPT nanoprodrug. (A) Oxidation and degradation of CPT prodrug CPT-TEG-ALA. (B) Recovered camptothecin from control and oxidized nanoprodrug after 24 and 48 h of dialysis. The prodrug was oxidized to 10, 25, or 50% of molar equivalent of CPT prodrug. Control nanoprodrug without oxidation. (*) $P < 0.02$, (**) $P < 0.002$, (***) $P < 0.001$. (C) Recovered α-tocopherol from control and oxidized nanoprodrug after 24 and 48 h of dialysis. (D) RP-HPLC chromatograms of the control and oxidized nanoprodrugs before (0 h) and after 24 and 48 h of incubation. P1, intact prodrug; P2, oxidized prodrug.

smaller than the size calculated by DLS method (~220 nm). This discrepancy is because DLS method is highly affected by the presence of a few larger particles, tending to be weighted to the larger particle sizes.[35] *In vitro* confocal fluorescence microscopic imaging demonstrated that U-87 MG glioma cells displayed effective cellular uptake after 5 h incubation with Cy5.5-labeled nanoprodrug (Figure 2C). Obviously, abundant nanoprodrugs were localized in the nuclei where CPT interacts with its cellular target topoisomerase I. In addition to the intracellular accumulation, nuclear localization plays a crucial role in the therapeutic efficacy of CPT nanoprodrug.

α-Lipoic acid is known to scavenge a wide range of ROSs and upon scavenge be converted into thiosulfinates and thiosulfonate (Figure 3A).[36] As part of the

prodrug, the oxidation of α-lipoic acid changes the structure and solubility of the prodrug, which may have great impact on the *in vivo* behavior of the drug. We hypothesized that the prodrug activation increases upon ROS scavenging, which is attributed to the increased hydrophilicity of the oxidized prodrug molecules. To demonstrate oxidation-sensitive prodrug activation, nanoprodrug was partially oxidized by addition of HOCl to 10, 25, or 50% of molar equivalent of CPT prodrug and the dependence of the rate of prodrug degradation on the degree of oxidation was monitored. The degraded CPT prodrugs were removed by dialysis and the amount of CPT prodrug remaining in the nanoprodrug was analyzed.

Figure 3B shows the total amount of CPT recovered after 24 and 48 h of incubation, regardless whether it is from the oxidized or intact prodrug. The amount of recovered CPT decreased with increasing degree of oxidation, indicating that more CPT prodrug was degraded from the oxidized nanoprodrug. About 62, 57, and 39% of the initial amount of CPT were recovered after 48 h from the nanoprodrug with 10, 25, or 50% of oxidation, respectively, while about 80% were recovered from control nanoprodrug without oxidation. Whereas the degradation of CPT prodrug is very sensitive to the presence of ROS, α-tocopherol remains practically unaffected by the oxidation (Figure 3C). The nonoxidized CPT prodrug remained relatively stable as shown in the control experiment (Figure 3D). About 97, 89, and 79% of the intact CPT prodrug were found before incubation ($t = 0$) after 24 and 48 h of incubation, respectively. More importantly for the concept of oxidation-sensitive nanoprodrug, the prodrug activation occurred mainly from oxidized prodrug (P2), while the intact prodrug (P1) was relatively stable. Comparing the integration of the peaks, the rate of degradation of the oxidized prodrug (k_2) was up to 10 times higher than the rate of the intact prodrug (k_1). The observed stability of α-tocopherol as a structural matrix plays a crucial role in the oxidation-sensitive nanoprodrug strategy. The oxidation of the nanoprodrug can occur practically everywhere in the body, for example, in the bloodstream and any body fluids. Therefore, it is very important to maintain the structural integrity until they reach the final target site without collapsing or disintegrating. The nanoprodrug maintained structural integrity when it was frozen and stored at −20 or −80 °C in the presence of 10% glucose (Figure S1), suggesting a cryoprotective effect of glucose during the freezing−thawing process. CPT prodrug remained intact during storage at −20 or −80 °C, whereas it oxidized considerably when stored at 4 °C or RT (Figure S2).

Characterization of Cellular Uptake of Nanoprodrug. Cellular uptake of nanomaterials largely depends on the particle size and surface characteristics, such as surface charge and hydrophobicity. Nanoparticles less than 200 nm in diameter can be internalized *via* several possible routes, including receptor mediated endocytosis, nonspecific, adsorptive endocytosis, and pinocytosis, while larger particles are internalized predominantly *via* caveolae-mediated endocytosis.[37] Most endocytosed nanoparticles are trapped in the endosomes and thus do not reach other cellular compartments in the cytosol unless there are endosomal disruptive or bypassing means are involved.[38,39] The fluorescence confocal images of U-87 glioma cells (Figure 2C) suggested that the nanoprodrug is not confined to vesicular endosomes but distributed throughout the cytosol of the cells. To explore the mechanism by which the nanoprodrug enters the cells, we analyzed internalization patterns of the nanoprodrug and compared with those of calcein. Calcein is a small molecule membrane-impermeable fluorophore and normally internalized *via* endocytic/pinocytic routes of cellular uptake. Cells were incubated in the presence of Cy5.5-labeled fluorescent nanoprodrug and calcein in serum-free or serum-containing medium for 1 h. Figure 4A shows that calcein was internalized by cells and displayed punctate fluorescence patterns indicative of endosomal uptake and localization in the endosomes, while a greater amount of nanoprodrugs were localized throughout the cytosol as a diffuse pattern of intracellular fluorescence overwhelming the punctuate pattern of calcein fluorescence, although few vesicular structures were observed for both the serum-free and serum-containing conditions. The nanoprodrug uptake and intracellular distribution were qualitatively similar in serum-free and serum-containing medium, indicating that nanoprodrugs are resistant to nonspecific protein adsorption and thus retain their behavior toward cell membranes.[40] Serum proteins did not change the size of nanoprodrug (Figure S3), suggesting that aggregation of nanoprodrugs or strong interaction with serum proteins did not occur. To further demonstrate the nonendocytic uptake of the nanoprodrugs, we carried out an immunofluorescence experiment to visually distinguish the endocytic pathway from the routes of the nanoprodrug internalization. U-87 glioma cells were incubated in the presence of fluorescent nanoprodrugs and then incubated with an early endosomal marker EEA-1 antibody. Figure 4B shows that the punctuate pattern of endosomes labeled with endosomal marker is very similar to the pattern of calcein uptake, consistent with the endocytic internalization mechanism of calcein, whereas the pattern of nanoprodrug fluorescence indicates that the nanoprodrugs were internalized most likely through nonendocytic pathways. The patterns of endosomes labeled with endosomal marker were qualitatively similar in serum-free and serum-containing medium, as the patterns of calcein uptake were. To obtain comparable fluorescence signals for calcein and the Cy5.5-labeled nanoprodrug, it was necessary to use

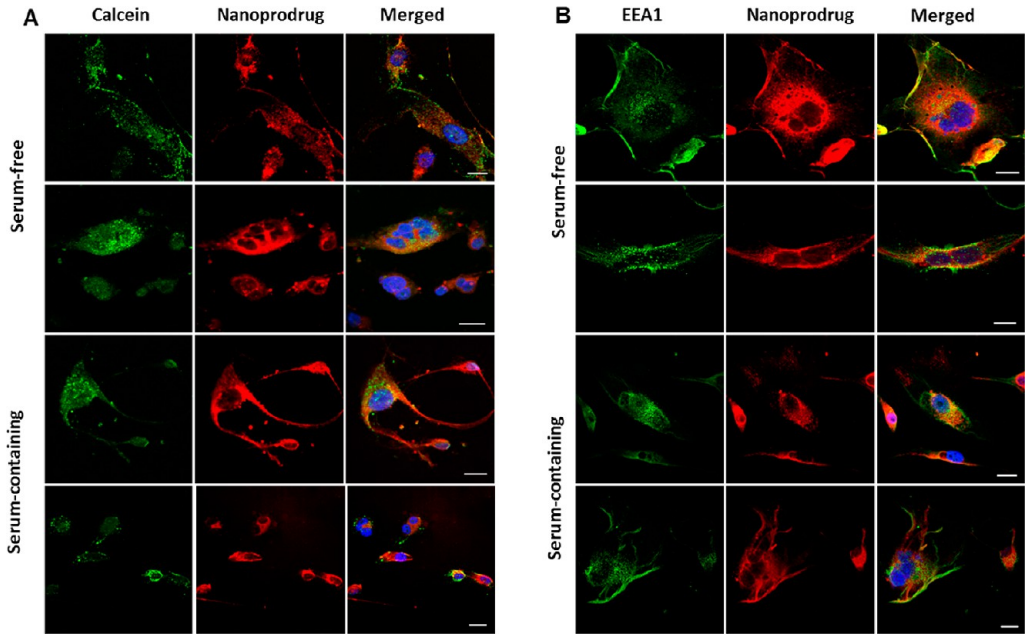

Figure 4. Characterization of cellular uptake of nanoprodrug into U-87 MG cells. (A) U-87 cells were incubated with calcein and nanoprodrug in serum-free and serum containing medium (10% FBS) at 37 °C and internalization was observed by confocal microscopy. Scale bar: 20 μm. (B) Confocal images of U-87 cells incubated with nanoprodrug in serum-free and serum containing medium (10% FBS) at 37 °C. The early endosomes were visualized in green by using the early endosome marker anti-EEA1 antibody. Nanoprodrug was visualized in red. Scale bar: 20 μm.

much higher concentration of calcein (200 μM) than Cy5.5 in the nanoprodrug (1 μM). Considering the fluorescence quantum yield of 0.38 for calcein and 0.2 for Cy5.5, the higher fluorescence intensity for the nanoprodrug can be explained that the nonendocytic internalization process is much more efficient than the endocytic process. Due to the intense and extensive distribution of fluorescence throughout the cytosol, it is not clear whether endocytic uptake of the nanoprodrug can be completely excluded. It is possible that nanoparticles can enter cells by a number of different routes. However, the observed patterns and intracellular distribution of the fluorescence clearly demonstrate that the majority of nanoprodrugs are internalized *via* direct penetration through plasma membrane rather than *via* a slower active endocytic pathway. The suggested direct penetration of nanomaterials through cell membrane has been previously observed in experiment with surface-modified gold nanoparticles or liposomes. Verma *et al.* reported that ~6 nm surface-modified gold nanoparticles penetrate the cell membrane bypassing endosomal routes.[41] Nativo *et al.* showed the endosomal route of cellular uptake of ~16 nm gold nanoparticles can be bypassed when the surface was modified with cell penetrating peptides or delivered by liposomes.[42] They suggested the existence of direct delivery routes across plasma membrane.

To further confirm the nonendocytic uptake of the nanoprodrug, we repeated the internalization experiments at 4 °C or in the presence of sodium azide/deoxyglucose to inhibit mechanisms of endocytic/pinocytic uptake. Figure 5 shows that the intensity and pattern of nanoprodrug fluorescence following the incubation at 4 °C or in the presence of sodium azide/deoxyglucose was indistinguishable from those of control experiment at 37 °C, whereas cells incubated with calcein at 4 °C or in the presence of sodium azide/deoxyglucose shows a negligible internalized dye. The uptake of the nanoprodrugs into the cytosol under conditions where endocytic routes are blocked confirms that the nanoprodrugs are capable of directly penetrating the cell membranes. In this study, we also observed that no escape of the internalized nanoprodrugs from cells occurred. Cells were incubated with calcein and nanoprodrug for 1 h, washed, and incubated for another 6 h without calcein and nanoprodrug. Figure 5B shows that calcein level dropped drastically, while the nanoprodrug fluorescence was qualitatively similar before and after the experiment. The results indicate that the level of calcein declines rapidly due to exocytosis of the dye entrapped in the endosomes and missing endocytosis following the removal of calcein from the medium. In general, the intracellular level of endocytosed nanoparticles declines rapidly when treatment is removed mainly due to exocytosis of the nanoparticles from cells.[43,44] The results again confirm the nonendocytic route of the nanoprodrug internalization. The observation also indicates that when the nanoprodrugs are in the cytosol they lose the structural characteristics necessary to pass through cell membranes,[41] and, thus, are unable to permeate cell membranes to exit out of cells. This phenomenon is of great importance

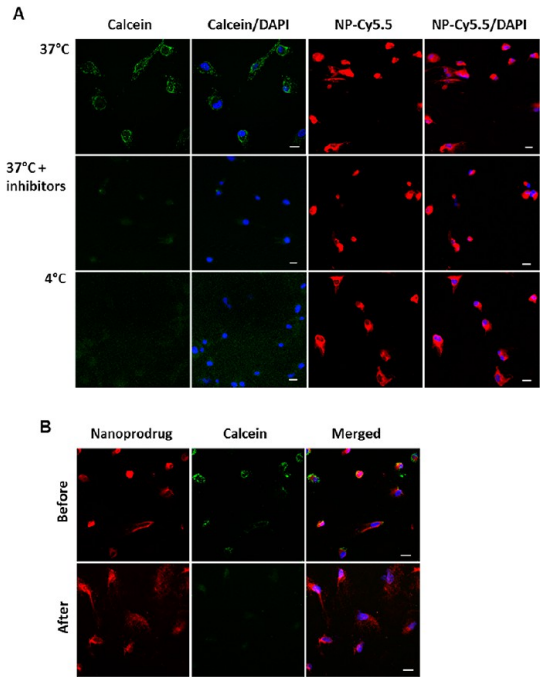

Figure 5. (A) U-87 cells were incubated with calcein and nanoprodrug for 1 h in serum-free medium at 37 °C (control), at 37 °C in the presence of inhibitors, and at 4 °C. The internalization of calcein or nanoprodrug was observed by confocal microscopy. At 4 °C or at the presence of inhibitor (deoxyglucose and sodium azide) the endocytic uptake of calcein was inhibited. The nanoprodrugs entered cells at 37 °C under conditions where active endocytic processes are blocked in the presence of inhibitors sodium azide and 2-deoxyglucose. Scale bar: 20 μm. (B) U-87 cells were incubated with calcein and nanoprodrug in serum-free medium at 37 °C for 1 h (before). The cells were then washed three times with fresh serum-free medium and incubated for 6 h in serum-free without calcein and nanoprodrug. Scale bar: 20 μm.

for cancer therapy. In general, drugs are cleared from the body within days after administration. To achieve optimal therapeutic efficacy, it is often necessary to maintain certain drug levels in the body. This necessitates more frequent or multiple dosing of drugs, which can cause considerable and frequent side effects. Therefore, enhanced internalization and sustained cellular retention of the nanoprodrug can reduce the burden of frequent dosing and severity of side effects.

***In Vivo* Accumulation of CPT Nanoprodrug in U-87 MG Tumor Xenograft.** To elucidate the targeting ability of the nanoprodrug *in vivo*, we examined the accumulation of fluorescent CPT nanoprodrug in subcutaneous and intracranial tumors. In the subcutaneous tumor model, fluorescent nanoprodrug was injected when the tumor size reached >1 cm. *In vivo* imaging was performed 72 h after the intravenous injection and organs were harvested. As shown in Figure 6A, the accumulation of the nanoprodrug occurred much stronger in the tumor tissue than in other organs. The signal intensity of the tumor was about 6.4, 2.3, 2.1, 11.7, 5.6, and 5.3 times higher than that of the brain, liver, kidney, heart, lung, and spleen, respectively (Figure 6B). No comparable accumulation occurred when injected with free Cy5.5 (Figure S4). The pattern of the fluorescence distribution in the dissected tumor tissue (Figure 6C) shows an enhanced nanoprodrug accumulation at the rapidly proliferating tumor boundaries. Figure 3C shows abnormal tumor vasculature immunostained with CD31 and brighter Cy5.5 fluorescence around the tumor blood vessels, suggesting that an extravasation of the nanoprodrug occurred across the wall of the tumor blood vessels. The intracellular delivery of the nanoprodrugs was evident with the high fluorescence around nuclei displayed as blue DAPI staining.

The targeted accumulation in tumor was further shown in the intracranial xenograft of U-87 MG glioma. *Ex vivo* fluorescence images of the tumor-bearing mice brains unambiguously demonstrated the accumulation of the nanoprodrug in the brain tumor (Figure 7A). While the fluorescence intensity of other organs changed only slightly, the signal intensity of the brain tumor increased about two and four times 24 and 48 h after nanoprodrug injection, respectively, suggesting a highly specific accumulation of the nanoprodrug in the brain tumor (Figure 7B). The signal intensity of the brain tumor area was about 10 times higher than that of the normal brain area. This feature highlights the ability of the CPT nanoprodrug to egress through the BBB in the tumor region but not in the healthy brain tissue surrounding the tumor. Notably, this discrimination between brain tumor and normal brain area was clearly shown 5 h after injection and became stronger. The ratio of fluorescence intensity of tumor to nontumor area in brain increased from 5.6 for 5 h to 12 and 16 for 24 and 48 h, respectively. In contrast, the fluorescence intensity of tumor rapidly decreased when injected with free Cy5.5 (Figure S5).

Rapid clearance of nanoparticles from the blood circulation and nonspecific biodistribution is a critical issue for the therapeutic efficacy and the potential for adverse side effects of nanoparticle drugs. Nanoparticles should be retained in the body at a sufficient concentration for a sufficient time to achieve therapeutic efficacy, whereas their long-term accumulation in organs may cause unfavorable side effects. If nanoparticles are smaller than 20 nm in diameter, they may undergo a rapid clearance *via* renal filtration, while larger nanoparticles (>200 nm) can be sequestered by sinusoids in spleen and fenestra of the liver.[45,46] If the sequestered nanoparticles are nonbiodegradable, long-term accumulation in the liver and spleen can occur, resulting in toxicity and negative side effects of the nanoparticles.[47] Larger nanoparticles can be removed by the mononuclear phagocytic systems (MPS). Phagocytic removal is carried out by a process known as opsonization. A protein known as opsonin adsorbs on the surface of nanoparticles in biological fluids, which promotes particle aggregation and recognition by the MPS in the liver and splenic filtration. This leads

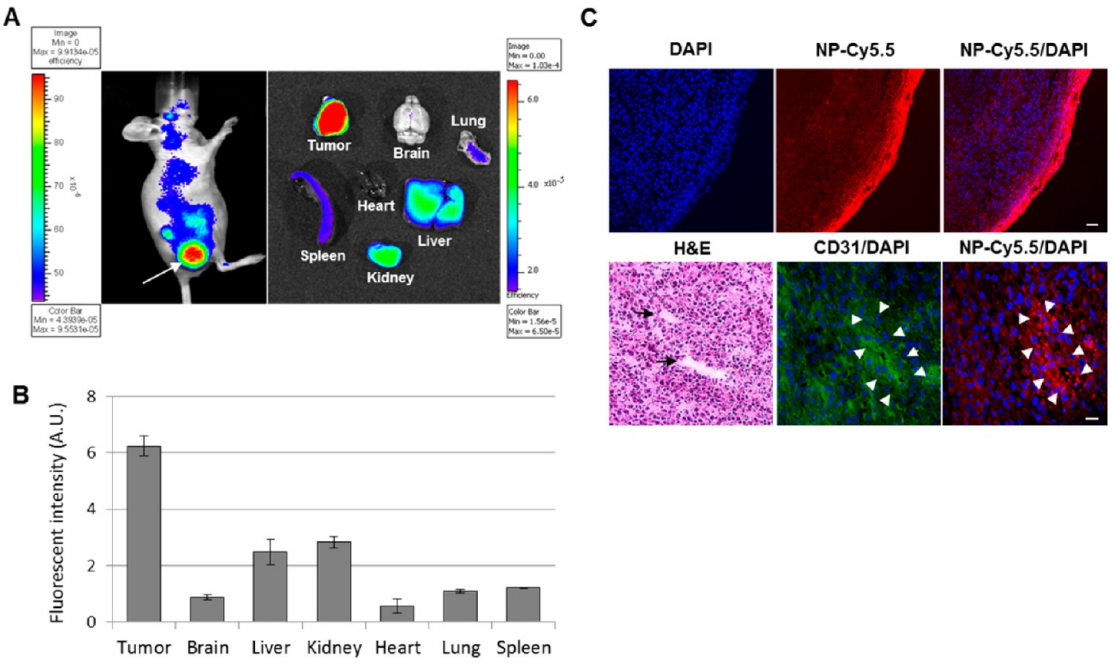

Figure 6. Biodistribution of Cy5.5-fluorescent CPT nanoprodrug in subcutaneous tumor. (A) Representative fluorescence images of mouse with subcutaneous U-87 MG glioma xenograft and organs harvested 72 h after intravenous injection of the fluorescent nanoprodrug. White arrow points to the tumor. (B) Relative fluorescence intensity of mouse organs from panel (A). Fluorescence intensity was quantified by measuring the signal intensity of equally sized areas of the tumor and organs in panel (A) using region of interest (ROI) tools of Xenogen 200 Imaging System. It shows means of three measurements of different areas. Bars, SD (C) U-87 MG subcutaneous xenograft tumor sections (10 μm) were stained with H&E, immunostained with CD31, or imaged for Cy5.5-fluorescent CPT nanoprodrug. The nuclei stained with DAPI are displayed in blue. Black and white arrows, tumor vasculature; scale bar: upper, 50 μm; down, 20 μm.

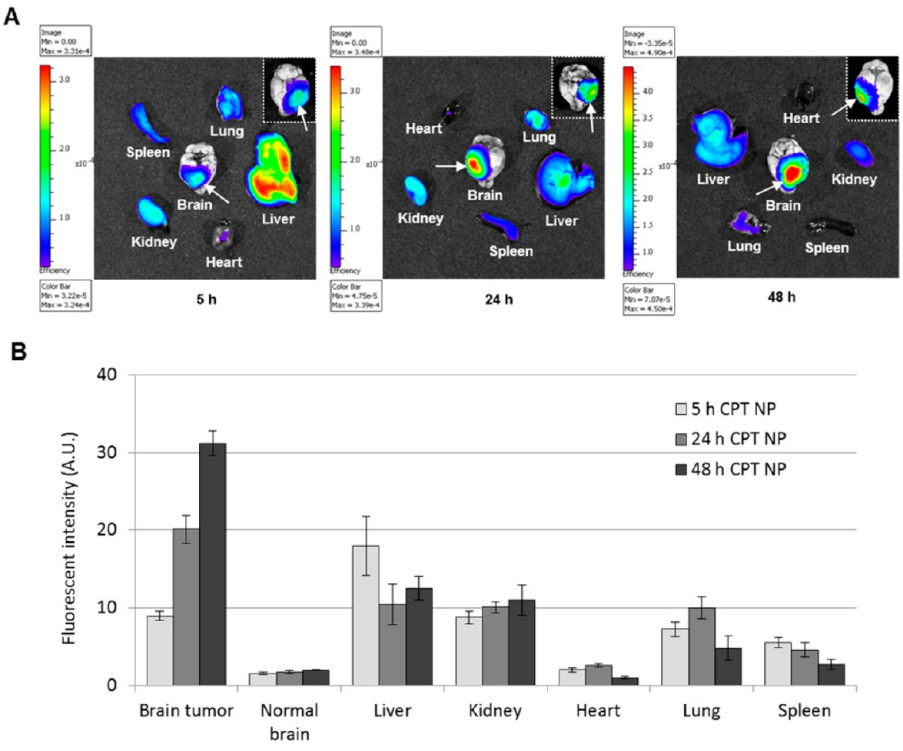

Figure 7. (A) Representative fluorescence images of brain and organs harvested from brain tumor-bearing mice 5, 24, and 48 h after intravenous injection of Cy5.5-fluorescent CPT nanoprodrug. (B) Fluorescence intensity was quantified by measuring the signal intensity of equally sized areas of the tumor and organs in panel (A) using region of interest (ROI) tools of Xenogen 200 Imaging System. It shows means of three measurements of different areas. Bars, SD. The reverse side of the brain was shown in white dotted rectangles. White arrows point to the tumors.

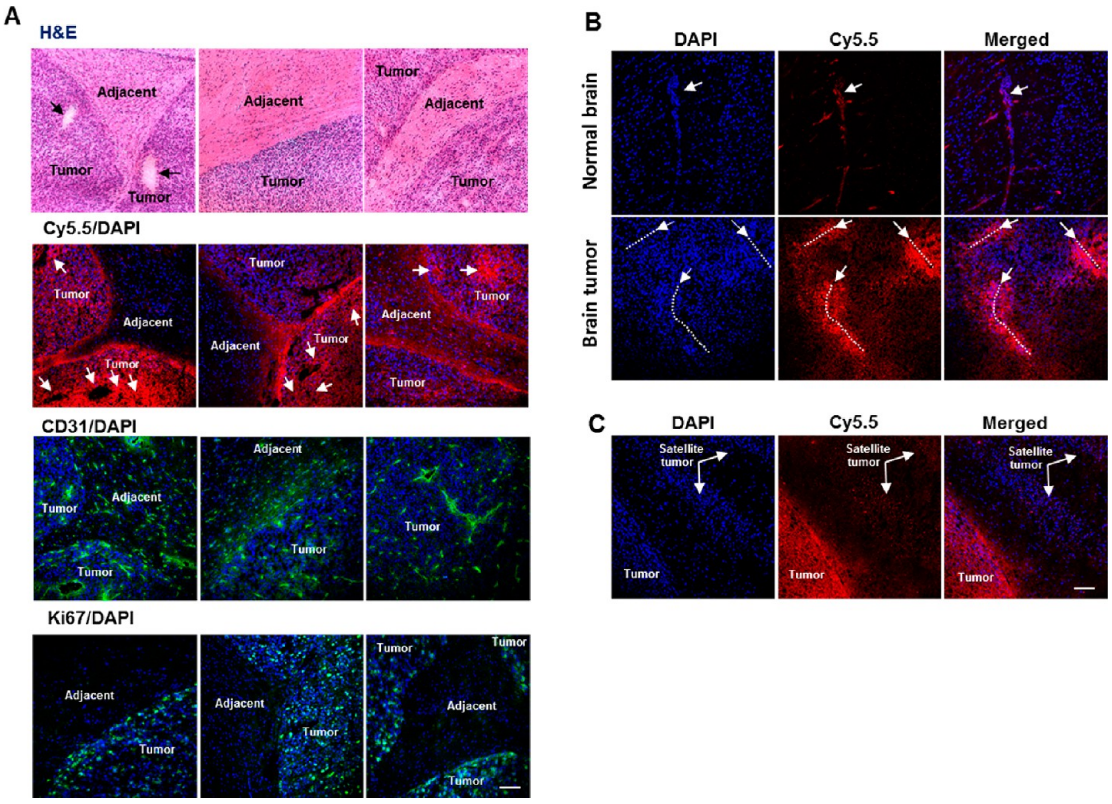

Figure 8. (A) Representative images of H&E staining, confocal Cy5.5 fluorescence, and CD31/Ki67 immunostaining of brain sections bearing U-87 MG intracranial tumor xenograft. The brain was harvested from brain tumor-bearing mouse 48 h after intravenous injection of Cy5.5-fluorescent CPT nanoprodrug. (B) The brain was harvested 24 h after intravenous injection of Cy5.5-fluorescent CPT nanoprodrug. White dotted line and arrow point to the blood vessels. (C) The brain was harvested 48 h after intravenous injection of Cy5.5-fluorescent CPT nanoprodrug. The nuclei stained with DAPI are displayed in blue. Scale bar: 100 μm.

to rapid clearance from the bloodstream.[48−50] Neutral nanoparticles have a much lower opsonization rate than charged particles.[51] Therefore, to minimize opsonization, nanoparticles are prepared to contain nonionic protecting shield molecules, most prominently PEG and PEG-containing copolymers such as poloxamers, poloxamines, and polysorbates.[52,53] The CPT nanoprodrug is a neutral system prepared using neutral CPT prodrug and α-tocopherol and nonionic surfactants minimizing interaction with charged biomolecules. We showed that serum proteins did not change the size of nanoprodrug (Figure S3) and did not influence the cellular uptake (Figure 4). As shown in Figure7, the nanoprodrug was detected in the liver, kidney, lung, and spleen 24 h after nanoprodrug administration. The intensity decreased for liver, lung, and spleen after 48 h, while it increased slightly for kidney, indicating a continuous renal clearance of degraded nanoprodrugs with a smaller diameter that could undergo renal filtration. α-Tocopherol makes more than 90% of the nanoprodrug. After hepatic uptake, α-tocopherol is preferentially secreted into the circulation and plays a key role in vitamin E recycling in the body.[54,55] α-Tocopherol and its oxidized metabolites are disposed of in the bile and ultimately excreted from the body.[56]

The pattern of the fluorescence distribution in the dissected brain tumor tissue (Figure 8) shows its ideal targeting property: strong accumulation confined to the tumor bed, no accumulation in adjacent healthy tissue, and maximum localization at the highly active, invading, tortuous tumor boundary. Ki67 positive cells were found with a higher density at the periphery of the tumor, confirming the known tendency of tumors to proliferate outward into healthy tissue.

These peripheral areas were also associated with areas of strong CD31 positive endothelial cells, indicating that the enhanced nanoprodrug accumulation preferably occurred at the rapidly proliferating tumor boundaries with strong tumor vasculature, suggesting optimal therapeutic efficacy of the nanoprodrug. Cancer stem cells have been shown to reside in the perivascular niche and this delivery pattern may specifically target this virulent subset of tumor cells.[57]

Compared with the blood vessels in normal brain tissue, the blood vessels in the tumor area are significantly larger and denser and have an increased permeability.[9,10] Figure 8B shows the extensive extravasation and distribution of fluorescent-labeled nanoprodrug from tumor blood vessels, whereas in the nontumor brain tissue, nanoprodrugs are mostly confined to blood vessels. Glioblastoma is one of the most

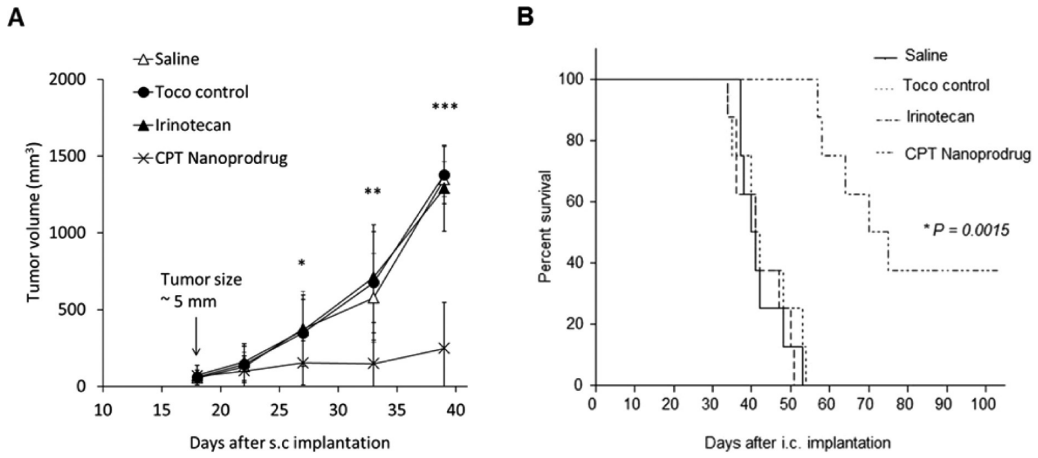

Figure 9. Antitumor efficacy of CPT nanoprodrug. (A) Volume of subcutaneous U-87 MG human tumor xenograft in mice after treatment with CPT nanoprodrug, irinotecan, α-tocopherol nanosuspension, and saline. Statistical significance was estimated by Student's *t*-test for the last three measurements of CPT nanoprodrug and saline control. (*) $P < 0.05$, (**) $P < 0.01$, (***) $P < 0.0001$. Points, means from six animals per group; bars, SD. (B) Kaplan–Meier survival plot demonstrating survival benefit of CPT nanoprodrug for animals with intracranial U-87 MG tumor xenograft. The figure shows percent survival of mice after treatment with CPT nanoprodrug, irinotecan, α-tocopherol nanosuspension, or saline. Statistical significance was estimated by log-rank method of CPT nanoprodrug compared with saline control.

aggressive and infiltrating tumors. While glioblastoma virtually never metastasizes out of the brain, it tends to spread (infiltrate) aggressively into adjacent tissues in the brain and form satellite tumors, the invasive islands of tumor cells.[58] Small satellite tumors can be easily overlooked and are extremely difficult to remove surgically. Their growth leads to the inevitable recurrence associated with the disease. Therefore, it is of great importance to target and delivery therapeutic agents to the satellite tumors. Figure 8C shows that the nanoprodrug is capable of targeting and accumulating in the satellite tumors.

***In Vivo* Efficacy of CPT Nanoprodrug.** In our previous report, we showed that the CPT nanoprodrug significantly inhibits proliferation of U-87 MG glioma cells.[27] In this study, we investigated the efficacy of the nanoprodrug on subcutaneous tumor growth of invasive U-87 MG cells (Figure 9A). Statistical analysis showed a significant reduction of tumor volume in the treatment group compared with saline and α-tocopherol control groups. The nanoprodrug inhibited tumor growth to about 250 mm^3 on day 21 after treatment, which was more than an 80% reduction compared with the control treatments (1350 mm^3).

It was of interest whether the nanoprodrug would be effective in a more clinically relevant orthotopic model of intracranially implanted U-87 MG cells. Figure 9B displays the result of a survival study of the mice with intracranial GBM xenograft. The median survival time was 72.5, 41.0, 40.5, and 41.5 days for CPT-TEG-ALA/Toco nanoprodrug, irinotecan, saline, and α-tocopherol nanosuspension, respectively. There were long-term survivors only in the nanoprodrug group (log rank, $P = 0.0015$).

Vigorous angiogenesis occurs to meet the tumor's accelerated metabolic need, resulting in defective vasculature with large pores and high permeability. The EPR effect has been clearly documented for most human solid tumors, including both primary and metastatic in nature.[9] Considering the dysfunctional brain tumor vasculature, we hypothesized that nanoparticle accumulation in a glioma model can be, like most solid tumor models, attributed to the EPR effect. Similarly, CPT nanoprodrug may be capable of passive targeting of brain tumor tissue *via* the EPR effect (Figure 10A). Cy5.5 fluorescence images of the whole brain and brain cut in OCT block unambiguously demonstrate that the accumulation of the nanoprodrug occurred in brain tumor, but not in healthy brain tissue. CD31 immunostaining shows a strong, abnormal vasculature in the tumor area and microvessels in normal brain tissue. Cy5.5 fluorescence images of the brain section show that CPT nanoprodrug was more localized around tumor blood vessels. Therefore, the accumulation of the nanoprodrug in the brain tumor is believed to be achieved by the passive tumor targeting accomplished by extravasation of the nanoprodrug through the compromised, hyperpermeable BTB and defective lymphatic drainage system in the brain tumor. Dysfunctional tumor vasculature often exhibits pores with cutoff sizes as large as 400–600 nm.[59] The U-87 human glioblastoma tumor model has shown high permeability when implanted in the cranial window of mice. It has been shown that the U-87 tumor was about two times more permeable to BSA compared with human colon cancer when implanted in the intracranial window of mice, although intracranial human colon cancer exhibited pore cutoff sizes of 380–550 nm, while U-87 human glioblastoma pore cutoff sizes were 7–100 nm.[60,61] This higher permeability was attributed to a comparatively higher frequency of open junctions in the U-87 tumor model. Therapeutically relevant upper limit of

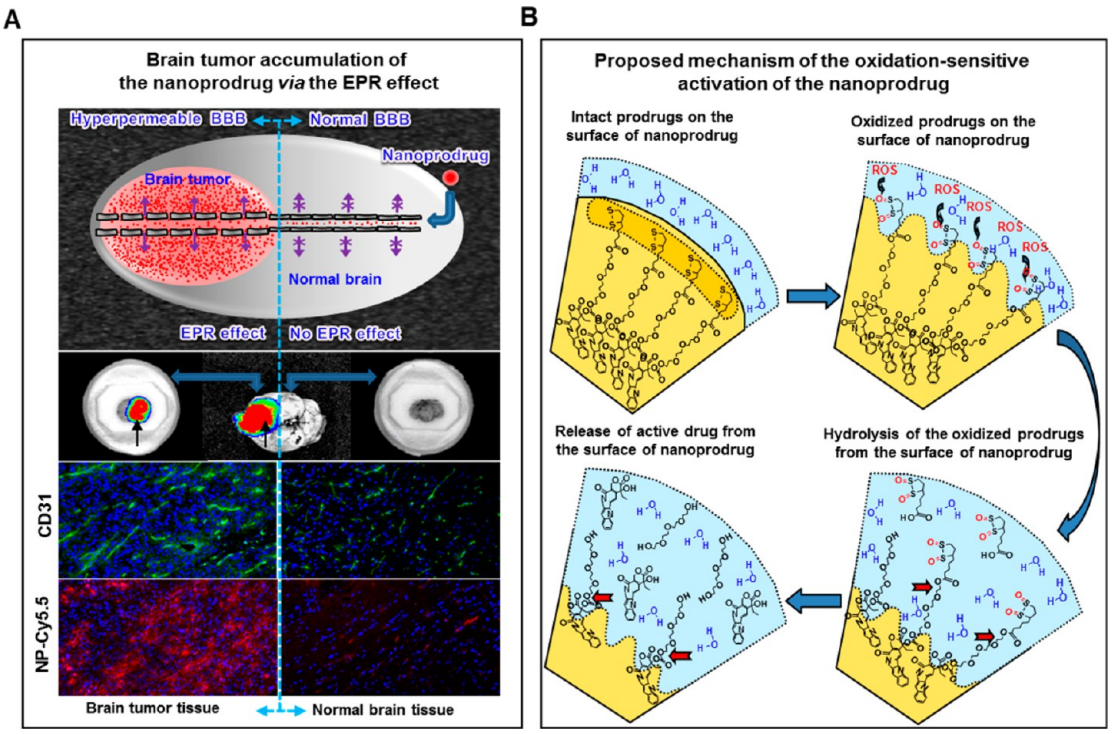

Figure 10. (A) Nanoprodrug accumulation *via* the enhanced permeability and retention (EPR) effect in the brain tumor tissue. Brain was harvested from brain tumor-bearing mouse 48 h after intravenous injection of fluorescent CPT nanoprodrug, cut as shown and frozen in OCT block. Black arrows point to the tumors. (B) Schematic representation of nanoprodrug activation in the oxidative environment of the brain tumor. α-Lipoic acid moiety of camptothecin prodrug scavenges ROS in the oxidative tumor microenvironment, accelerating the erosion of the nanoprodrug surface. This facilitates the hydrolytic or enzymatic degradation of the prodrug. Red arrow shows the site of hydrolysis.

the BBB pore size has been reported to range between 20 and 100 nm.[62] The size of the nanoprodrug used in the study was measured to be around 200 nm by the dynamic light scattering (DLS) and around 150 nm by the nanoparticle tracking and analysis (NTA) technique, which is considerably larger than the reported cut-off size. Therefore, a more thorough understanding of the factors at work that allow for such remarkable *in vivo* accumulation must be pursued.

The highly specific accumulation of the nanoprodrug in tumor tissues followed by efficient intracellular uptake may be of importance for the treatment of cancers developing resistance to anticancer therapeutics, denoted multidrug resistance (MDR). MDR mediated by P-glycoprotein (Pgp) is the best characterized mechanism of MDR in brain tumors. Pgp has been found to be expressed in the cell membrane of brain tumor cells and in the endothelial cells of newly formed brain tumor blood vessels.[63] This integral membrane transporter protein reduces intracellular drug levels by inhibiting drug uptake and promoting drug efflux. The use of nanoparticles that enter the cells by endocytosis may overcome Pgp-mediated MDR. It has been suggested that Pgp recognizes hydrophobic drugs when they are present in the plasma membrane, but not when they are already in the cytoplasm.[64] Therefore, nanoparticles that enter the cells without releasing drugs in the membrane may overcome the Pgp-mediated MDR. The superior anticancer efficacy of CPT nanoprodrug compared with irinotecan may be attributed to the increased level of therapeutic drug in the tumor cells, which is accomplished by the combination of the passive accumulation of the nanoprodrug in the tumor tissue (EPR effect) and efficient cellular uptake *via* nonendocytic cell membrane permeation. This combined effect may contribute to overcoming Pgp-mediated MDR for the nanoprodrug, allowing drug accumulation in the cytoplasm, whereas both irinotecan and its active metabolite SN38 are substrates of Pgp.[65,66] It is important to note that the selective tumor accumulation, intracellular uptake, and nuclear localization of the nanoprodrug are necessary factors leading to its remarkable therapeutic efficacy. The mechanism and efficiency of the nuclear localization of the nanoprodrug is not yet clear and require further research. In addition, we plan to evaluate the effect of this nuclear localization on the therapeutic efficacy of the nanoprodrug. This knowledge will provide insight into the antitumor action of the nanoprodrug.

The nanoprodrug contains two antioxidant components: α-tocopherol as a structural matrix and α-lipoic acid as part of the CPT prodrug. α-Tocopherol is the most relevant form of vitamin E and believed to be the most potent lipid-soluble antioxidant that can break the propagation of the free lipid radical chain reaction in the biological membrane. There have been increasing

data that vitamin E may play a role in the prevention and treatment of oxidative damage-related diseases in the brain.[67] As a structural matrix, α-tocopherol reduced the size and increased chemical and physical stability of nanoprodrugs, which is ascribed to enhanced structural integrity of the nanoprodrugs by means of strong hydrophobic assembly of α-tocopherol.[68] The other antioxidant component, α-lipoic acid moiety of the CPT prodrug, serves as a molecular switch of the nanoprodrug that scavenges a number of ROS and undergoes structural change, leading to enhanced prodrug activation. We previously characterized the CPT nanoprodrug with regard to structure, reactive oxygen species (ROS) scavenging capability, enzymatic activation, release kinetics, and *in vitro* anticancer efficacy against U-87 MG glioma cells.[34] We demonstrated that the α-lipoic acid moiety efficiently scavenged ROS, leading to accelerated destabilization of the nanoprodrug and increased prodrug activation.[69] This suggests that the nanoprodrug is activated preferably in an oxidative environment, including the highly inflammatory tumor microenvironment. The oxidative destabilization has been attributed to the increased hydrophilicity of the oxidized prodrugs on the surface of the nanoprodrug; the oxidized, hydrophilic prodrugs extrude into the aqueous environment, allowing enzymatic degradation of the prodrugs (Figure 10B). In this way, more prodrugs are degraded in an accelerated fashion by esterases as oxidation occurs on the surface of the nanoprodrug in the tumor microenvironment. This unique interaction between oxidative destabilization and enzymatic prodrug activation characterizes the oxidative stimuli-responsive nanoprodrug. ROS have been reported to be directly involved in the link between chronic inflammation and cancer. Inflammation is widely recognized to be a critical component of tumor progression, survival, and migration by virtue of recruiting and stimulating inflammatory cells, generating abundant ROS.[70,71] There is considerable evidence that ROS play a major role in tumor initiation and progression in both animal models and humans.[72,73] It has been reported that reducing inflammation in the tumor microenvironment inhibits tumor progression in a mouse model.[74]

Tumor microenvironment is characterized by hypoxia (low levels of O_2). Paradoxically, the production of ROS is increased under hypoxic conditions. When the oxygen level decreases, the electron transport chain of the mitochondria senses the hypoxic condition and responds by releasing ROS.[75] It has been proposed that a low level of oxygen itself and ROS generated as byproducts are involved in the stabilization and activation of hypoxia-inducible factor 1 (HIF1), which in turn increases the energy production by glycolysis, while the energy production by mitochondria decreases.[76,77] This metabolic shift in energy generation is believed to facilitate tumor survival in a hypoxic tumor environment.[78] Metabolic deprivation and hypoxia caused by extensive tumor growth stimulate cells in the periphery of the primary tumor to become invasive and infiltrate normal brain tissue.[58] It has also been reported that hypoxia promotes metastasis of cancer cells and attenuation of ROS by antioxidants suppressed hypoxia-induced metastasis of cancer cells.[79] Metabolic deprivation and hypoxia caused by extensive tumor growth stimulate cells in the periphery of the primary tumor to become invasive and infiltrate normal brain tissue. Thus, the combined effect of the oxidation-sensitive activation and capability of accumulating in the more actively proliferating tumor periphery and satellite tumors makes the nanoprodrug an ideal tumor-targeting therapeutic agent.

CONCLUSION

In summary, the ability of the nanoprodrug to pass through the BBB and selectively accumulate in the brain tumor is a valuable property for brain tumor therapy. Importantly, the accumulation was achieved by passive drug targeting to tumors *via* the EPR effect without using active targeting ligands such as tumor-specific peptides or antibodies. The nanoprodrug entered cells *via* nonendocytic cell membrane permeation, which was found much more efficient than endocytic routes and was retained within the cells, leading to a sustained cellular drug accumulation. Consequently, a similar therapeutic effect can be achieved with less drug dosing and side effects. The nanoprodrug strategy is a versatile method of developing therapeutic nanoparticles by converting drugs into prodrugs and transforming them into nanoprodrugs. In addition, the nanoprodrug system may also be used as a safe, low-cost, and targeted delivery vehicle, being capable of delivering hydrophobic agents in the matrix and hydrophilic agents on the surface. Therefore, nanoprodrugs represent a universal vehicle for targeted cancer therapy. We believe that the implications of this discovery are significant in the field of cancer therapy, and ongoing research into targeted cancer therapy using nanoprodrugs will further define the mechanism of tumor-specific delivery and prodrug activation.

MATERIALS AND METHODS

Chemicals and Reagents. All chemicals were analytical grade unless otherwise specified. α-Tocopherol, acetone, polysorbate 80, Pluronic F68, 1-octadecanethiol, 2-deoxy-D-glucose, calcein, sodium azide, sodium citrate, NaCl, paraformaldehyde (PFA), sodium hypochlorite, hematoxylin, eosin, dialysis tubing cellulose membrane (D9777), irinotecan, esterase (E3019), monoclonal anti-EEA1 antibody (E7659), FITC-conjugated goat antimouse IgG,

FITC-conjugated goat antirat IgG, and FITC-conjugated goat antirabbit IgG was obtained from Sigma-Aldrich (St Louis, MO); Triton X-100 from Fisher Scientific (BP151); betadine solution (10% povidone-iodine) from Purdue Frederick, Stamford, CT; ketamine from Bioniche Teoranta, Galway, Ireland; atipamezole and dexmedetomidine from Orion Corporation, Espoo, Finland; Carprofen from Hospira, Lake Forest, IL; Isoflurane from Piramal Critical Care, Bethlehem, PA; buprenorphine from Reckitt Benckiser Pharmaceuticals, Richmond, VA; hydrophilic syringe filter from Corning (Corning, NY); Minium Essential Medium (MEM), fetal bovine serum (FBS), penicillin, streptomycin, phosphate buffered saline (PBS), mounting medium with DAPI (Prolong Gold), and rabbit antihuman K_i-67 (polyclonal) from Invitrogen (Carlsbad, CA); rat antimouse CD31 (Clone MEC 13.3) and four chamber culture slides from BD Biosciences (San Jose, CA); Cy5.5 maleimide and MicroSpin G-25 Sephadex column from GE Healthcare (Piscataway, NJ); Cy5.5 carboxylic acid from Lumiprobe (Hallandale Beach, FL); OCT compound from Sakura (Torrance, CA); and Hamilton syringe from Hamilton (Reno, NV).

Synthesis of Camptothecin Prodrug and Nanoprodrug Preparation. CPT prodrug was synthesized by introducing biodegradable ester and carbonate bonds as described in Figure 1. Nanoprodrugs were prepared according to the method using spontaneous emulsification with multistep modification. For a single-step procedure, 7 mg of CPT-TEG-ALA and 50 mg α-tocopherol were dissolved in acetone (5 mL) containing polysorbate 80 (0.1% w/v). The organic solution was poured under moderate stirring on a magnetic plate into an aqueous phase prepared by dissolving 25 mg of Pluronic F68 in 10 mL of distilled water (0.25% w/v). Following 15 min of magnetic stirring, the acetone was removed under reduced pressure. For a multistep procedure, the emulsification/evaporation cycle was repeated three times. The nanoprodrug suspension obtained from the first emulsification/evaporation cycle was used as the aqueous phase for the second emulsification, and so forth. The suspension was dialyzed in cellulose membrane tube overnight in distilled water and filtered consecutively through 0.8, 0.45, and 0.2 μm hydrophilic syringe filter and stored at 4 °C. α-Tocopherol control nanosuspension was prepared using the same procedure, except for the omission of CPT prodrug. The hydrodynamic size of the nanoprodrug was measured by the dynamic light scattering (DLS) using a Coulter N4-Plus Submicrometer Particle Sizer. For the visualization and size measurement of the nanoprodrugs, Nanoparticle Tracking Analysis (NTA) was performed using a digital microscope LM10 system (Nanosight, Amesbury, U.K.).[35]

Fluorescent Labeling of the Nanoprodrug. Cy5.5-labeled CPT nanoprodrug was prepared using a single-step procedure, as described above, except that 2 mg of 1-octadecanethiol was added to the organic phase. To 2 mL of the suspension of 1-octadecanethiol-containing nanoprodrugs, 500 μL of 10× PBS and 1.1 mol equiv of Cy5.5 maleimide were added. The reaction mixture was incubated overnight at room temperature under light protection. To remove unbound Cy5.5 maleimide, the suspension was purified on a MicroSpin G-25 Sephadex column equilibrated with 20 mM sodium citrate buffer with 0.15 M NaCl.[80] The labeled nanoprodrug was filtered and stored, as described above. The concentration of the bound Cy5.5 was determined as follows: 50 μL of the labeled nanoprodrug suspention was mixed with 950 μL DMSO and the absorbance was measured at 675 nm. The concentration was calculated using a standard curve generated with Cy5.5 maleimide.

Oxidation-Sensitive Prodrug Activation. To demonstrate oxidation-sensitive prodrug activation, nanoprodrug was partially oxidized and the rate of prodrug activation was monitored. The partial oxidation was performed by adding hypochlorous acid (HOCl) to the nanoprodrug suspension to give the final concentration of 10, 25, and 50% of molar equivalent of CPT prodrug. The concentration of HOCl in the diluted commercial sodium hypochlorite solution was determined spectrophotometrically (ε_{292} = 350 M^{-1} cm^{-1}).[81] After addition of HOCl, the nanoprodrug suspension was incubated for 30 min at 37 °C, transferred into dialysis membrane (Sigma, D9777) and then dialyzed in water for 48 h. Samples were taken after 24 and 48 h and analyzed using RP-HPLC. RP-HPLC analysis was performed on a Merck-Hitachi analytical LaChrom D-7000 HPLC/UV detector system (Merck, Darmstadt, Germany) with a CAPCELL PAK, Type SG 120 (Phenomenex, Torrance, CA, U.S.A.) C_{18} reversed phase column (250/4.6 mm, 5 μm). To analyze the composition of the nanoprodrug suspension, 200 μL of the nanoprodrug suspension was mixed with 350 μL of acetonitrile and then analyzed using RP-HPLC. The composition of the mobile phase (acetonitrile/water mixture containing 0.1% (v/v) trifluoroacetic acid) was adjusted for oxidized and nonoxidized prodrug in order to provide an appropriate retention time and separation. To determine the total amount of camptothecin available from the nanoprodrug after 24 and 48 h of dialysis, the aqueous nanoprodrug suspension (200 μL) was incubated in the presence of 25 μL of 10× PBS and 25 μL of esterase (20 U/mL) for 30 min at 37 °C. The reaction mixture (250 μL) was mixed with 250 μL of acetonitrile, centrifuged for 2 min at 20000 × g, and then analyzed using RP-HPLC. The separation was performed under isocratic condition with a 60/40 mixture of acetonitrile/water at a flow rate of 1 mL/min. The detection was carried out at 360 nm.

***In Vitro* Cell Culture and Uptake of Nanoprodrugs.** The human glioblastoma cell line U-87MG was obtained from American Type Culture Collection (ATCC, Bethesda, MD, U.S.A.). The cells were tested and authenticated by the providers and maintained according to the provider's instruction. The cumulative culture length of the cells was <2 months after reception. The cells were grown and maintained in Minimum Essential Medium (MEM) containing antibiotics penicillin (100 U/mL) and streptomycin (100 μg/mL) and supplemented with 10% fetal bovine serum. Cells were grown at 37 °C at an atmosphere of 5% CO_2 in humidified air. To demonstrate intracellular uptake, cells were incubated in the presence of Cy5.5-labeled nanoprodrug at a final concentration of 1 μM Cy5.5. Four chamber culture slides were seeded with U-87 cells, and the cells were allowed to attach for 24 h. The medium was replaced with 1.0 mL of freshly prepared suspension of the fluorescent-labeled nanoprodrug in medium, and the chamber slides were incubated for 5 h. Cells were washed three times with PBS to remove free nanoprodrug, one drop of mounting medium with DAPI was added, and then cover slides were placed. To study the mechanism of cellular uptake of the nanoprodrug, cells were incubated with nanoprodrug and calcein, and the pattern of cellular uptake was observed. Cells were grown in a four-chamber culture slide overnight, and then medium was exchanged with fresh serum-free or serum-containing (10% FBS) MEM medium. For a study in serum-free medium at 37 °C, the attached cells were washed three times with prewarmed serum-free medium and preincubated in serum-free medium for 30 min at 37 °C. Fluorescent nanoprodrug was added at a final concentration of 1 μM Cy5.5. Calcein was added at a final concentration up to 200 μM. The cells were incubated at 37 °C for 1h, washed three times with prewarmed PBS, and then slides for confocal analysis were prepared as described above. For studies at 4 °C, the cells were preincubated at 4 °C for 30 min before nanoprodrug and calcein addition. The serum-free medium, solutions for washes, nanoprodrug suspension, and calcein solution were all preincubated to 4 °C before use. Samples incubated with both calcein and nanoprodrug were also studied. To study the cellular uptake of nanoprodrug after blockage of endocytosis, the cells were incubated with 10 and 50 mM of sodium azide and 2-deoxyglucose, respectively, for 30 min at 37 °C. Then, calcein (200 μM) or nanoprodrug (1 μM Cy5.5) was added and the cells were incubated for another 30 min. The cells were then washed with PBS and slides were prepared as described above. For microscopic analysis, a confocal laser-scanning microscope (Leica Microsystem SP5, Mannheim, Germany) equipped with a digital camera with a fluorescence microscope (Model Upright Zeiss, Jena, Germany) was used.

Animal Model. All animal studies were performed according to Cedars-Sinai Medical Center Institutional Animal Care and Use Committee protocols. Female 6- to 8-week-old immunodeficient athymic nu/nu nude mice (Crl:Nu-*Foxn1*^{nu}, Charles River Laboratories) were used for all experiments. For subcutaneous tumor model, 10^7 U-87 MG human glioma cells suspended in PBS (100 uL) were injected in the right flank under anesthesia

with Isoflurane (3% to effect). For an intracranial tumor model, mice underwent intracranial stereotactic implantation of U-87 MG cells. Mice were anesthetized using a ketamine (75 mg/kg) and dexmedetomidine (0.5 mg/kg) combination as a single intraperitoneal injection. Betadine solution (10% povidone-iodine) was used to prepare the skin at the incision site on the skull. After anesthesia induction and prior to surgery, Carprofen (4 mg/kg) was administered subcutaneously in upper left arm to aid in the management of postoperative pain. A skin incision was made, a hole was drilled in the skull, and 5×10^4 U-87 MG cells suspended in 2 μL of PBS were implanted in the right frontal region of the brain, 2 mm to the right of Bregma and 3.0 mm of depth, using a Hamilton syringe. The animals were injected with atipamezole (1 mg/kg) intraperitoneally to reverse the dexmedetomidine effect and are allowed to recover from anesthesia. A single subcutaneous injection of buprenorphine (0.1 mg/kg) was administered for pain relief.

***In Vivo* Antitumor Efficacy of Nanoprodrug.** The antitumor effect of the CPT nanoprodrug was tested on subcutaneous and intracranial xenografts of U-87 MG tumors in mice. In the subcutaneous model, treatment was started when the tumor size reached approximately 0.5−1.0 cm in diameter. The animals ($n = 6$) received intravenous (tail vein) injection of nanoprodrug on a daily basis for five days (4 mg/kg/day CPT-TEG-ALA). Two perpendicular diameters of the tumor were measured, and the volume was calculated according to the following equation: $V\,(\mathrm{mm}^3) = L\,(\mathrm{mm}) \times W^2\,(\mathrm{mm}^2)/2$, where L is the longest diameter and W is the diameter perpendicular to L. In the intracranial model, the animals ($n = 8$) received intravenous (tail vein) injection of nanoprodrug (16 mg/kg/day CPT-TEG-ALA) beginning 7 days after tumor implantation every three days for 4 weeks. As control, animals received injection of irinotecan, α-tocopherol nanosuspension, or saline. The injection was performed under anesthesia with Isoflurane (3% to effect).

Optical Imaging. In the subcutaneous model, 100 μL of fluorescent nanoprodrug (10 μM Cy5.5) were injected (tail vein) when the tumor reached >1 cm. In the intracranial model, fluorescent nanoprodrug was injected when there were signs of significant neurological impairment. Fluorescence imaging of the living animals and harvested organs were performed using Xenogen 200 Imaging System (Caliper Life Sciences). Organs (brain, heart, liver, kidney, spleen, and lung) were harvested from the animals and imaged immediately. Imaging was made on the whole body (subcutaneous model only), isolated tumors and organs, and tumor sections embedded and frozen in OCT compound. For fluorescence confocal microscopy, tumors were cryosectioned with a thickness of 10 μm (Leica CM3050S), one drop of mounting medium with DAPI was added, and then cover slides were placed. For microscopic analysis, a confocal laser-scanning microscope (Leica Microsystem SP5, Mannheim, Germany) equipped with a digital camera with a fluorescence microscope (Model Upright Zeiss) was used.

Histology and Immunohistochemistry. Whole brains were harvested immediately after the animals were sacrificed, frozen in OCT compound, cryosectioned (10 μm), and stained with hematoxylin and eosin. For immunohistochemistry, sections were fixed in 4% PFA for 5 min. Slides were washed three times by gentle shaking in PBS and blocked for 1 h in 10% goat serum in PBS. To demonstrate tumor angiogenesis, the slides were incubated with rat antimouse CD31 diluted 1:50 in 0.5% goat serum in PBS for 1 h at room temperature followed by three times wash in PBS. The slides were then incubated with FITC-conjugated goat antirat IgG diluted 1:100 in 0.5% goat serum in PBS for 1 h at room temperature followed by three times wash in PBS. To detect the proliferative activity, sections were treated with rabbit antihuman K_i-67 diluted 1:100 and then FITC-conjugated goat antirabbit IgG diluted 1:100 as described above. To study the endocytic internalization, cells were incubated in the presence of nanoprodrug and calcein and then reacted with an early endosome marker EEA-1. Cells were grown in four chamber slides, fixed in 4% PFA for 5 min, and then washed three times by gentle shaking in PBS. Cells were permeabilized with 0.1% Triton-X 100 in PBS for 10 min and washed three times with PBS. Cells were blocked for 1 h in 10% goat serum in PBS at room temperature. The cells were then incubated with mouse anti-EEA1 antibody diluted 1:100 in 0.5% goat serum in PBS for 1 h at room temperature followed by three times wash in PBS. The slides were then incubated with FITC-conjugated goat antimouse IgG diluted 1:100 in 0.5% goat serum in PBS for 1 h at room temperature followed by three times wash in PBS. Slides were prepared as described above. All sections were counterstained with DAPI by adding one drop of mounting medium with DAPI. Confocal microscopic analysis was performed as described above.

Statistical Analysis. Other than the survival study, the results were analyzed and expressed as mean ± standard deviation (S.D.). Statistical analysis of the results was carried out using Student's *t*-test. For the mouse survival study, log-rank statistical analysis was performed. For all tests, differences were considered statistically significant at $P < 0.05$.

Conflict of Interest: The authors declare no competing financial interest.

Acknowledgment. The authors wish to thank Dr. J. Young and members from the Department of Comparative Medicine, Cedars-Sinai Medical Center, for support and advice with animals.

Supporting Information Available: Stability of CPT nanoprodrug under various storage conditions, influence of serum proteins on CPT nanoprodrug size, and comparison of biodistribution of CPT nanoprodrug and free Cy5.5 dye. This material is available free of charge *via* the Internet at http://pubs.acs.org.

REFERENCES AND NOTES

1. Krex, D.; Klink, B.; Hartmann, C.; von Deimling, A.; Pietsch, T.; Simon, M.; Sabel, M.; Steinbach, J. P.; Heese, O.; Reifenberger, G.; et al. Long-Term Survival with Glioblastoma Multiforme. *Brain* **2007**, *130*, 2596–2606.
2. Yang, I.; Aghi, M. K. New Advances That Enable Identification of Glioblastoma Recurrence. *Nat. Rev. Clin. Oncol.* **2009**, *6*, 648–657.
3. Cecchelli, R.; Berezowski, V.; Lundquist, S.; Culot, M.; Renftel, M.; Dehouck, M. P.; Fenart, L. Modelling of the Blood−Brain Barrier in Drug Discovery and Development. *Nat. Rev. Drug Discovery* **2007**, *6*, 650–661.
4. Hawkins, B. T.; Davis, T. P. The Blood−Brain Barrier/Neurovascular Unit in Health and Disease. *Pharmacol. Rev.* **2005**, *57*, 173–185.
5. Juillerat-Jeanneret, L. The Targeted Delivery of Cancer Drugs across the Blood−Brain Barrier: Chemical Modifications of Drugs or Drug-Nanoparticles? *Drug Discovery Today* **2008**, *13*, 1099–1106.
6. Wolburg, H.; Wolburg-Buchholz, K.; Kraus, J.; Rascher-Eggstein, G.; Liebner, S.; Hamm, S.; Duffner, F.; Grote, E. H.; Risau, W.; Engelhardt, B. Localization of Claudin-3 in Tight Junctions of the Blood−Brain Barrier is Selectively Lost during Experimental Autoimmune Encephalomyelitis and Human Glioblastoma Multiforme. *Acta Neuropathol.* **2003**, *105*, 586–592.
7. Zlokovic, B. V. The Blood−Brain Barrier in Health and Chronic Neurodegenerative Disorders. *Neuron* **2008**, *57*, 178–201.
8. Shlosberg, D.; Benifla, M.; Kaufer, D.; Friedman, A. Blood−Brain Barrier Breakdown as a Therapeutic Target in Traumatic Brain Injury. *Nat. Rev. Neurol.* **2010**, *6*, 393–403.
9. Iyer, A. K.; Khaled, G.; Fang, J.; Maeda, H. Exploiting the Enhanced Permeability and Retention Effect for Tumor Targeting. *Drug Discovery Today* **2006**, *11*, 812–818.
10. Maeda, H. The Enhanced Permeability and Retention (EPR) Effect in Tumor Vasculature: The Key Role of Tumor-Selective Macromolecular Drug Targeting. *Adv. Enzyme Regul.* **2001**, *41*, 189–207.
11. Wall, M. E.; Wani, M. C.; Cook, C. E.; Palmer, K. H.; McPhail, H. T.; Sim, G. A. Plant Antitumor Agents. I. The Isolation and Structure of Camptothecin, a Novel Alkaloidal Leukemia and Tumor Inhibitor from Camptotheca Acuminate. *J. Am. Chem. Soc.* **1966**, *88*, 3888–3890.
12. Wani, M. C.; Ronman, P. E.; Lindley, J. T.; Wall, M. E. Plant Antitumor Agents. 18. Synthesis and Biological Activity of Camptothecin Analogs. *J. Med. Chem.* **1980**, *23*, 554–560.

13. Pizzolato, J. F.; Saltz, L. B. The Camptothecins. *Lancet* **2003**, *361*, 2235–2242.
14. Gottlieb, J. A.; Luce, J. K. Treatment of Malignant Melanoma with Camptothecin (NSC-100880). *Cancer Chemother. Rep., Part I* **1972**, *56*, 103–105.
15. Muggia, F. M.; Creaven, P. J.; Hanson, H. H.; Cohen, M. C.; Selawry, O. S.; Phase, I. Clinical Trial of Weekly and Daily Treatment with Camptothecin (NSC-100880): Correlation with Preclinical Studies. *Biochemistry* **1972**, *56*, 515–521.
16. Moertel, C. G.; Schutt, A. J.; Reitemerer, R. G.; Hahn, R. G. Phase II Study of Camptothecin (NSC-100880) in the Treatment of Advanced Gastrointestinal Cancer. *Cancer Chemother. Rep., Part I* **1972**, *56*, 95–101.
17. Hsiang, Y. H.; Hertzberg, R.; Hecht, S.; Liu, L. F. Camptothecin Induces Protein-Linked DNA Breaks *via* Mammalian DNA Topoisomerase I. *J. Biol. Chem.* **1985**, *260*, 14873–14878.
18. Lorence, A.; Nessler, C. L. Camptothecin, Over Four Decades of Surprising Findings. *Phytochemistry* **2004**, *65*, 2735–2749.
19. Greenwald, R. B.; Pendri, A.; Conover, C.; Gilbert, C.; Yang, R.; Xia, J. Drug Delivery Systems. 2. Camptothecin 20-*O*-Poly(Ethylene Glycol) Ester Transport Forms. *J. Med. Chem.* **1996**, *39*, 1938–1940.
20. Singer, J. W.; Bhatt, R.; Tulinsky, J.; Buhler, K. R.; Heasley, E.; Klein, P.; de Vries, P. Water-Soluble Poly-(L-Glutamic Acid)-Gly Camptothecin Conjugates Enhance Camptothecin Stability and Efficacy *In Vivo*. *J. Controlled Release* **2001**, *74*, 243–247.
21. Harada, M.; Sakakibara, H.; Yano, T.; Suzuki, T.; Okuno, S. Determinants for the Drug Release from T-0128, Camptothecin Analogue-Carboxymethyl Dextran Conjugate. *J. Controlled Release* **2000**, *69*, 399–412.
22. Ferrari, M. Cancer Nanotechnology: Opportunities and Challenges. *Nat. Rev. Cancer* **2005**, *5*, 161–171.
23. Kuo, F.; Subramanian, B.; Kotyla, T.; Wilson, T. A.; Yoganathan, S.; Nicolosi, R. J. Nanoemulsions of an Anti-Oxidant Synergy Formulation Containing Gamma Tocopherol Have Enhanced Bioavailability and Anti-Inflammatory Properties. *Int. J. Pharm.* **2008**, *363*, 206–213.
24. Noble, C. O.; Krauze, M. T.; Drummond, D. C.; Yamashita, Y.; Saito, R.; Berger, M. S.; Kirpotin, D. B.; Bankiewicz, K. S.; Park, J. W. Novel Nanoliposomal CPT-11 Infused by Convection-Enhanced Delivery in Intracranial Tumors: Pharmacology and Efficacy. *Cancer Res.* **2006**, *66*, 2801–2806.
25. Lyer, L.; King, C. D.; Whitington, P. F.; Green, M. D.; Roy, S. K.; Tephly, T. R.; Coffman, B. L.; Ratain, M. J. Genetic Predisposition to the Metabolism of Irinotecan (CPT-11). Role of Uridine Diphosphate Glucuronosyltransferase Isoform 1A1 in the Glucuronidation of Its Active Metabolite (SN-38) in Human Liver Microsomes. *J. Clin. Invest.* **1998**, *101*, 847–854.
26. Koizumi, F.; Kitagawa, M.; Negishi, T.; Onda, T.; Matsumoto, S.; Hamaguchi, T.; Matsumura, Y. Novel SN-38–Incorporating Polymeric Micelles, NK012, Eradicate Vascular Endothelial Growth Factor–Secreting Bulky Tumors. *Cancer Res.* **2006**, *66*, 10048–10056.
27. Lee, B. S.; Nalla, A. K.; Stock, I. R.; Shear, T. C.; Black, K. L.; Yu, J. S. Oxidative Stimuli-Responsive Nanoprodrug of Camptothecin Kills Glioblastoma Cells. *Bioorg. Med. Chem. Lett.* **2010**, *20*, 5262–5268.
28. Acharya, S.; Sahoo, S. K. PLGA Nanoparticles Containing Various Anticancer Agents and Tumour Delivery by EPR Effect. *Adv. Drug Delivery Rev.* **2011**, *63*, 170–183.
29. McCarron, P. A.; Marouf, W. M.; Quinn, D. J.; Fay, F.; Burden, R. E.; Olwill, S. A.; Scott, C. J. Antibody Targeting of Camptothecin-Loaded PLGA Nanoparticles to Tumor Cells. *Bioconjugate Chem.* **2008**, *19*, 1561–1569.
30. Emerson, D. L. Liposomal Delivery of Camptothecin. *Pharm. Sci. Technol. Today* **2000**, *3*, 205–209.
31. Sawyer, A. J.; Saucier-Sawyer, J. K.; Booth, C. J.; Liu, J.; Patel, T.; Piepmeier, J. M.; Saltzman, W. M. Convection-Enhanced Delivery of Camptothecin-Loaded Polymer Nanoparticles for Treatment of Intracranial Tumors. *Drug Delivery Transl. Res.* **2011**, *1*, 34–42.
32. Whitesides, G. M.; Mathias, J. P.; Seto, C. T. Molecular Self-Assembly and Nanochemistry: A Chemical Strategy for the Synthesis of Nanostructures. *DTIC Technical Report, No. 45*; DTIC: Ft. Belvoir, VA, **1991**.
33. Whitesides, G. M.; Grzybowski, B. Self-Assembly at All Scales. *Science* **2002**, *295*, 2418–2421.
34. Shafiq, S.; Shakeel, F.; Talegaonkar, S.; Ahmad, F. J.; Khar, R. K.; Ali, M. Development and Bioavailability Assessment of Ramipril Nanoemulsion Formulation. *Eur. J. Pharm. Biopharm.* **2007**, *66*, 227–243.
35. Filipe, V.; Hawe, A.; Jiskoot, W. Critical Evaluation of Nanoparticle Tracking Analysis (NTA) by NanoSight for the Measurement of Nanoparticles and Protein Aggregates. *Pharm. Res.* **2010**, *27*, 796–810.
36. Biewenga, G. Ph.; de Jong, J.; Bast, A. Lipoic Acid Favors Thiosulfinate Formation After Hypochlorous Acid Scavenging: A Study with Lipoic Acid Derivatives. *Arch. Biochem. Biophys.* **1994**, *312*, 114–120.
37. Rejman, J.; Oberle, V.; Zuhorn, I. S.; Hoekstra Size-Dependent Internalization of Particles *via* the Pathways of Clathrin- and Caveolae-Mediated Endocytosis. *Biochem. J.* **2004**, *377*, 159–169.
38. Shukla, R.; Bansal, V.; Chaudhary, M.; Basu, A.; Bhonde, R. R.; Sastry, M. Biocompatibility of Gold Nanoparticles and Their Endocytotic Fate inside the Cellular Compartment: A Microscopic Overview. *Langmuir* **2005**, *21*, 10644–10654.
39. Hu, Y.; Litwin, T.; Nagaraja, A. R.; Kwong, B.; Katz, J.; Watson, N.; Irvine, D. J. Cytosolic Delivery of Membrane-Impermeable Molecules in Dendritic Cells Using pH-Responsive Core-Shell Nanoparticles. *Nano Lett.* **2007**, *7*, 3056–3064.
40. Jackson, A. M.; Myerson, J. W.; Stellacci, F. Spontaneous Assembly of Subnanometre-Ordered Domains in the Ligand Shell of Monolayer-Protected Nanoparticles. *Nat. Mater.* **2004**, *3*, 330–336.
41. Verma, A.; Uzun, O.; Hu, Y.; Hu, Y.; Han, H.; Watson, N.; Chen, S.; Irvine, D. J.; Stellacci, F. Surface Structure-Regulated Cell Membrane Penetration by Monolayer Protected Nanoparticles. *Nat. Mater.* **2008**, *7*, 588–595.
42. Nativo, P.; Prior, I. A.; Brust, M. Uptake and Intracellular Fate of Surface-Modified Gold Nanoparticles. *ACS Nano* **2008**, *2*, 1639–1644.
43. Panyam, J.; Labhasetwar, V. Dynamics of Endocytosis and Exocytosis of Poly(D,L-lactide-*co*-glycolide) Nanoparticles in Vascular Smooth Muscle Cells. *Pharm. Res.* **2003**, *20*, 212–220.
44. Sahoo, S. K.; Labhasetwar, V. Enhanced Antiproliferative Activity of Transferrin-Conjugated Paclitaxel-Loaded Nanoparticles is Mediated *via* Sustained Intracellular Drug Retention. *Mol. Pharmaceutics* **2005**, *2*, 373–383.
45. Venturoli, D.; Rippe, B. Ficoll and Dextran *vs* Globular Proteins as Probes for Testing Glomerular Permselectivity: Effects of Molecular Size, Shape, Charge, and Deformability. *Am. J. Physiol. Renal Physiol.* **2005**, *288*, F605–613.
46. Yuan, F. Transvascular Drug Delivery in Solid Tumors. *Semin. Radiat. Oncol.* **1998**, *8*, 164–175.
47. Moghimi, S. M.; Porter, C. J. H.; Muir, I. S.; Illum, L.; Davis, S. S. Non-Phagocytic Uptake of Intravenously Injected Microspheres in Rat Spleen: Influence of Particle Size and Hydrophilic Coating. *Biochem. Biophys. Res. Commun.* **1991**, *177*, 861–866.
48. Owens, D. E., III; Peppas, N. A. Opsonization, Biodistribution, and Pharmacokinetics of Polymeric Nanoparticles. *Int. J. Pharm.* **2006**, *307*, 93–102.
49. Romberg, B.; Hennink, W. E.; Storm, G. Sheddable Coatings for Long-Circulating Nanoparticles. *Pharm. Res.* **2008**, *25*, 55–71.
50. Alexis, F.; Pridgen, E.; Molnar, L. K.; Farokhzad, O. C. Factors Affecting the Clearance and Biodistribution of Polymeric Nanoparticles. *Mol. Pharmaceutics* **2008**, *5*, 505–515.
51. Roser, M.; Fischer, D.; Kissel, T. Surface-Modified Biodegradable Albumin Nano- and Microspheres. II. Effect of Surface Charges on *In Vitro* Phagocytosis and Biodistribution in Rats. *Eur. J. Pharm. Biopharm.* **1998**, *46*, 255–263.
52. Illum, L.; Hunneyball, I. M.; Davis, S. S. The Effect of Hydrophilic Coatings on the Uptake of Colloidal Particles by the Liver and by Peritoneal Macrophages. *Int. J. Pharm.* **1986**, *29*, 53–65.

53. Plard, J. P.; Bazile, D. Comparison of the Safety Profiles of PLA(50) and Me.PEG-PLA(50) Nanoparticles After Single Dose Intravenous Administration to Rat. *Colloids Surf., B* **1999**, *16*, 173–183.
54. Kaempf-Rotzoll, D. E.; Traber, M. G.; Arai, H. Vitamin E and Transfer Proteins. *Curr. Opin. Lipidol.* **2003**, *14*, 249–254.
55. Traber, M. G.; Arai, H. Molecular Mechanisms of Vitamin E Transport. *Annu. Rev. Nutr.* **1999**, *19*, 343–355.
56. Mustacich, D. J.; Shields, J.; Horton, R. A.; Brown, M. K.; Reed, D. J. Biliary Secretion of Alpha Tocopherol and the Role of the Mdr2 P-Glycoprotein in Rats and Mice. *Arch. Biochem. Biophys.* **1998**, *350*, 183–192.
57. Gilbertson, R. J.; Rich, J. N. Making a Tumour's Bed: Glioblastoma Stem Cells and the Vascular Niche. *Nat. Rev. Cancer* **2007**, *7*, 733–736.
58. Rubenstein, J. L.; Kim, J.; Ozawa, T.; Zhang, M.; Westphal, M.; Deen, D. F.; Shuman, M. A. Anti-VEGF Antibody Treatment of Glioblastoma Prolongs Survival but Results in Increased Vascular Cooption. *Neoplasia* **2000**, *2*, 306–314.
59. Yuan, F.; Dellian, M.; Fukumura, D.; Leunig, M.; Berk, D. A.; Torchilin, V. P.; Jain, R. K. Vascular Permeability in a Human Tumor Xenograft: Molecular Size Dependence and Cutoff Size. *Cancer Res.* **1995**, *55*, 3752–3756.
60. Yuan, F.; Salehi, H. A.; Boucher, Y.; Vasthare, U. S.; Tuma, R. F.; Jain, R. K. Vascular Permeability and Microcirculation of Gliomas and Mammary Carcinomas Transplanted in Rat and Mouse Cranial Windows. *Cancer Res.* **1994**, *54*, 4564–4568.
61. Hobbs, S. K.; Monsky, W. L.; Yuan, F.; Roberts, W. G.; Griffith, L.; Torchilin, V. P.; Jain, R. K. Regulation of Transport Pathways in Tumor Vessels: Role of Tumor Type and Microenvironment. *Proc. Natl. Acad. Sci. U.S.A.* **1998**, *95*, 4607–4612.
62. Sarin, H.; Kanevsky, A. S.; Wu, H.; Brimacombe, K. R.; Fung, S. H.; Sousa, A. A.; Auh, S.; Wilson, C. M.; Sharma, K.; Aronova, M. A.; et al. Effective Transvascular Delivery of Nanoparticles Across the Blood−Brain Tumor Barrier into Malignant Glioma Cells. *J. Transl. Med.* **2008**, *6*, 80.
63. Bredel, M.; Zentner, J. Brain-Tumour Drug Resistence: The Bare Essentials. *Lancet Oncol.* **2002**, *3*, 397–406.
64. Shapiro, A. B.; Corder, A. B.; Ling, V. P-Glycoprotein-Mediated Hoechst 33342 Transport Out of the Lipid Bilayer. *Eur. J. Biochem.* **1997**, *250*, 115–121.
65. Iyer, L.; Ramírez, J.; Shepard, D. R.; Bingham, C. M.; Hossfeld, D. K.; Ratain, M. J.; Mayer, U. Biliary Transport of Irinotecan and Metabolites in Normal and P-Glycoprotein-Deficient Mice. *Cancer Chemother. Pharmacol.* **2002**, *49*, 336–341.
66. Jansen, W. J.; Hulscher, T. M.; van Ark-Otte, J.; Giaccone, G.; Pinedo, H. M.; Boven, E. CPT-11 Sensitivity in Relation to the Expression of P170-Glycoprotein and Multidrug Resistance-Associated Protein. *Br. J. Cancer* **1998**, *77*, 359–365.
67. Gilgun-Sherki, Y.; Melamed, E.; Offen, D. Oxidative Stress Induced-Neurodegenerative Disease: The Need for Antioxidants That Penetrate the Blood−Brain Barrier. *Neuropharmacology* **2001**, *40*, 959–975.
68. Lee, B. S.; Yoon, C. W.; Osipov, A.; Moghaven, N.; Nwachokor, D.; Amatya, R.; Na, R.; Pantoja, J. L.; Pham, M. D.; Black, K. L.; Yu, J. S. Nanoprodrugs of NSAIDs: Preparation and Characterization of Flufenamic Acid Nanoprodrugs. *J. Drug Delivery* **2011**, ID 980720:13.
69. Lee, B. S.; Yuan, X.; Xu, Q.; McLafferty, F. S.; Petersen, B. A.; Collette, J. C.; Black, K. L.; Yu, J. S. Stimuli-Responsive Antioxidant Nanoprodrugs of NSAIDs. *Int. J. Pharm.* **2009**, *372*, 112–124.
70. Ohshima, H.; Bartsch, H. Chronic Infections and Inflammation Process as Cancer Risk Factors: Possible Role of Nitric Oxide in Carcinogenesis. *Mutat. Res.* **1994**, *305*, 253–264.
71. Weitzman, S. A.; Gordon, L. I. Inflammation and Cancer: Role of Phagocyte-Generated Oxidants in Carcinogenesis. *Blood* **1990**, *76*, 655–663.
72. Trush, M. A.; Kensler, T. W. An Overview of the Relationship between Oxidative Stress and Chemical Carcinogenesis. *Free Radical Biol. Med.* **1991**, *10*, 201–209.
73. Cerutti, P. A. Prooxidant States and Tumor Promotion. *Science* **1985**, *227*, 375–381.
74. Bunt, S. K.; Yang, L.; Sinha, P.; Clements, V. K.; Leips, J.; Ostrand-Rosenberg, S. Reduced Inflammation in the Tumor Microenvironment Delays the Accumulation of Myeloid-Derived Suppressor Cells and Limits Tumor Progression. *Cancer Res.* **2007**, *67*, 10019–10026.
75. Guzy, R. D.; Schumacker, P. T. Oxygen Sensing by Mitochondria at Complex III: The Paradox of Increased ROS during Hypoxia. *Exp. Physiol.* **2006**, *91*, 807–819.
76. Stiehl, D. P.; Wirthner, R.; Köditz, J.; Spielmann, P.; Camenisch, G.; Wenger, R. H. Increased Prolyl-4-hydroxylase Domain Proteins Compensate for Decreased Oxygen Levels. Evidence for an Autoregulatory Oxygen-Sensing System. *J. Biol. Chem.* **2006**, *281*, 23482–23491.
77. Chandel, N. S.; McClintock, D. S.; Feliciano, C. E.; Wood, T. M.; Melendez, J. A.; Rodriguez, A. M.; Schumacker, P. T. Reactive Oxygen Species Generated at Mitochondrial Complex III Stabilize Hypoxia-Inducible Factor-1α during Hypoxia: A Mechanism of O_2 Sensing. *J. Biol. Chem.* **2000**, *275*, 25130–25138.
78. Denko, N. C. Hypoxia, HIF1 and Glucose Metabolism in the Solid Tumour. *Nat. Rev. Cancer* **2008**, *8*, 705–713.
79. Shimojo, Y.; Akimoto, M.; Hisanaga, T.; Tanaka, T.; Tajima, Y.; Honma, Y.; Takenaga, K. Attenuation of Reactive Oxygen Species by Antioxidants Suppresses Hypoxia-Induced Epithelial-Mesenchymal Transition and Metastasis of Pancreatic Cancer Cells. *Clin. Exp. Metastasis* **2013**, *30*, 143–154.
80. Kircher, M. F.; Mahmood, U.; King, R. S.; Weissleder, R.; Josephson, L. A Multimodal Nanoparticle for Preoperative Magnetic Resonance Imaging and Intraoperative Optical Brain Tumor Delineation. *Cancer Res.* **2003**, *63*, 8122–8125.
81. Morris, C. J. The Acid Ionization Constant of HOCl from 5 to 35 °C. *J. Phys. Chem.* **1966**, *70*, 3798–3805.